

## Review

# State-of-the-art of selective laser melting process: A comprehensive review



Eyob Messele Sefene

Faculty of Mechanical and Industrial Engineering, Bahir Dar Institute of Technology, Bahir Dar University, P.O. Box 26, Bahir Dar, Ethiopia

## ARTICLE INFO

**Keywords:**

Additive Manufacturing  
Selective Laser Melting  
Materials  
Process parameters  
Support structures  
FEA

## ABSTRACT

In recent times, smart manufacturing systems and materials are being utilized increasingly for producing parts with high strength-to-weight ratios. Consolidation of several assembly parts into a single and lightweight component plays a vital role in enhancing the mechanical properties of systems as well as effective energy conservation in several sectors, including aviation, maritime, and automotive industries. Additive Manufacturing (AM) has enabled the manufacturing of lightweight components by depositing materials only when needed and significantly reduce required assemblies. From the different AM technologies, Selective Laser Melting (SLM) is a prominent process used to fabricate near-net-shape and good surface quality parts using metal, ceramic, and polymer materials. The potential of realizing customized complex metallic structures with applications in the biomedical, transportation, and energy industries has piqued the interest of the scientific society in SLM. Although substantial progress has been achieved in comprehending the SLM process and fabricating different materials with this process, however, the industrial application is still restricted. Limitations related to printing of multi-materials, inadequate information on the efficient process parameters for different materials, and porosities on the printed parts are some of the main hurdles buried in this method that prevent it from manufacturing functional parts. Therefore, this review article provides a comprehensive and state-of-the-art study on the SLM process regarding the types of materials used, the printing of reflective material and multi-materials, the effect of several process parameters on thermo-mechanical properties of parts, printing of lattice structure, a novel support structure technique, types of post-processing methods, and basic information on simulation software used for SLM processes. Moreover, the article describes future prospects and suggests research directions for the SLM process.

## 1. Introduction

Industry 4.0 has taken a tremendous stride in the production system, data management, and cybersecurity integrating smart technologies and production systems in this modern age. Among these, additive manufacturing plays an essential role in meeting some of the essential requirements of the fourth industrial revolution [1,2]. Additive Manufacturing (AM) is one of the suitable manufacturing techniques for producing any part geometries by accumulating single or multi-materials selectively with a layer-by-layer or particle-by-particle fashion directly from the digital data model (CAD file) [3–8]. The entire workflow of AM, described in Fig. 1, instigates creating a model using various types of CAD software and ends with complete the part printing and post-processing [9–12]. Among the most notable endowments in the AM process include reducing overall cost, weight, and assembly parts by modifying the component shape and getting a higher strength-to-weight ratio [13]. In this contemporary era, countless businesses in aerospace [14], biomedical [15], automotive [16], turbomachinery [17], food [18], and other manufacturing industries are interested in utilizing AM processes due to its lightweight

higher-strength ratio characteristics, minimizing manufacturing lead time, and an easy process for customization of the customer needs. [19–21]. Several processes are categorized under AM process. According to the ASTM F-42 standard illustrated in Fig. 1, AM process is classified into seven major categories [22,23]. One of the processes that proffer numerous possible benefits from the seventh AM category is the Powder Bed Fusion (PBF) process. The process is among the ones which are getting increasing attention as an emerging polymer and metal AM technology, and it uses laser or electron beam as an energy source for fusing or melting the powder materials to create parts layer by layer. [24]. PBF processes are categorized into beam-based PBF, which requires a high energy beam, and non-beam (heater/lamp)-based PBF, which does not require a high energy beam. Selective Laser Sintering (SLS), Selective Laser Melting (SLM), and Electron Beam Melting (EBM) are examples of beam-based PBF processes. The beam-based PBF process is classified into two groups: Laser beam-based PBF (L-PBF, which comprises SLS and SLM processes), and electron beam PBF process included EBM process [25]. Under the L-PBF category, Selective Laser Melting (SLM) is a renowned [26,27] AM process that produces near-net-shape parts with good mechanical properties, surface finish

<https://doi.org/10.1016/j.jmansy.2022.04.002>

Received 14 August 2021; Received in revised form 31 March 2022; Accepted 1 April 2022

Available online 9 April 2022

0278-6125/© 2022 The Society of Manufacturing Engineers. Published by Elsevier Ltd. All rights reserved.

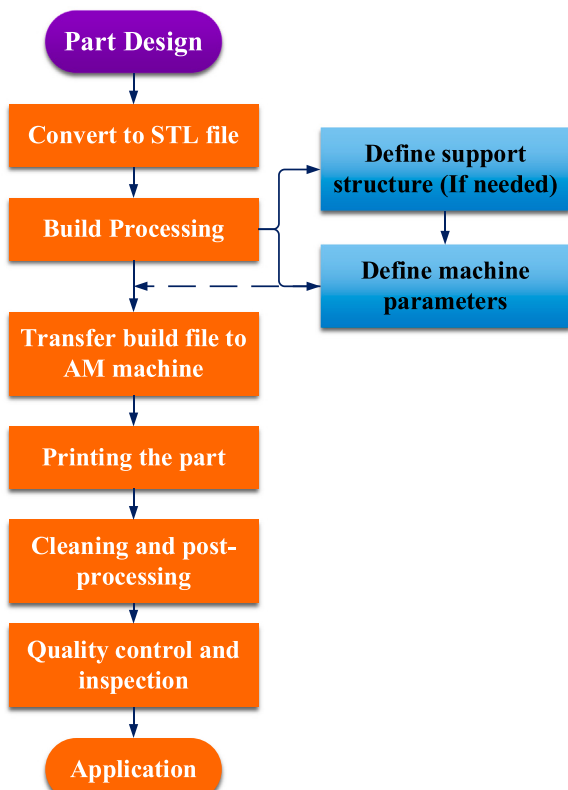


Fig. 1. Basic workflow of AM [9–11].

appearance, and complex geometries [28,29]. The process is appropriate for fabricating the multifaceted parts with a higher density up to 99.9% by melts the metallic powders via a high-power-density laser. The working principle of the SLM process illustrated in Fig. 3 initiates by applying a thin powder layer into the building platform, then the applied powder wholly melted on the thermal energy induced by one or several laser beams [30–33]. Due to its mechanical property and lightweight characteristics, the demand for utilization of the SLM process is swiftly increased in several industries, including aerospace, automotive, electronic, chemical, biomedical, and other high-tech areas [34,35]. One of the most applicable SLM processes in the aerospace industry is to make aircraft mechanical parts out of various materials, comprising steel, Ti alloys, and Ni-based superalloys. Moreover, these processes can minimize the number of assembly parts into a single component, and the weight of the part can also be optimized [36]. Meanwhile, residual stress and shrinkages are critical phenomena in the SLM process. The laser power enlarges the material during the process, and it will contract the laser power has been removed. In addition to this, the residual stress also occurred due to the utilization of improper process parameters [37].

In order to produce a high-quality printed product, three prominent aspects of the printing process must be considered: firstly, the properties of powder materials (virgin or recycled, and particle size), process parameters (correlation of one parameter to the other one), and prediction of stresses using FE software are crucial [38]. In addition, the use of materials must be compatible with the printed part design. There is a possibility of applying different materials such as metals and their alloys, ceramics, bioactive glass, polymers, and their combinations of fabricating different geometries for various applications. Those material characteristics in the SLM process are compatible with the required designs. Besides, the use of virgin powder imparts good mechanical properties compared to recycled one, and particle size is a significant parameter on the relative density and strength properties [39,40]. Secondly, using appropriate process parameters with materials can minimize defects such as porosity, incomplete fusion holes, and cracks. Even

though the mechanical properties of the printed part highly depend on the process parameters. Zhang, et al. [41] studied the defect formations in the SLM process, and they concluded that the energy density process parameters could control defects in the SLM process. Additionally, scan strategy is also a significant parameter for minimizing the location distribution defects. Most of the defects are found at the scan track endpoint and between two adjacent tracks. Thirdly, finite element software can be used to predict and control the molten pool size, temperature gradients, and stresses generated by the employed process parameters during the depositing of a single layer of the material [42]. Some of the significant drawbacks of the SLM process are porosity and shrinkage on the printed part resulting from inappropriate process parameters [43]. To minimize these drawbacks, parameter optimization, understanding the effects of a single parameter, and selecting materials significantly contribute. Hence, this study presents a comprehensive review of the work done on the advancements to date instigates from material utilization to simulation software for the SLM process has been reviewed.

## 2. Materials

AM process can determine the characteristics of powder material precursors. The main criteria for the selection of metal and ceramic powders used in the AM process are grain shape (spherical, irregular, granulated), see Fig. 4, composition (pre-alloyed or mixed), gas infusions, powder followability, propensity to oxidize, and sintering/melting conditions [46]. Powder particle size and shapes are pretty critical for determining the mechanical property of the printed part. The research investigations that have been done to study the influence of particle size on powder properties are summarized in Table 1. Besides, the powder materials' chemical composition and purity level are vital in selecting powder materials for the AM process. Balbaa, et al. [47] studied the effect of fine and coarse powder particle size on the L-PBF process using AlSi10Mg alloy materials. Their findings revealed that the fine powder particle size imparts the minimum density (due to higher oxygen) and lower dimensional accuracy. On the other hand, the lower surface roughness was observed at the coarse powder particle compared to the fine. Popov, et al. [46] compiled four years (2011, 2013, 2017, and 2020) of Critical Raw Materials (CRMs) that are especially pertinent in the field of biomedicine, aerospace, electric vehicles, and energy application materials that are processed by modern manufacturing technologies, including AM techniques, marked in different colors as shown in Fig. 5. The materials such as metals and ceramics are identified for AM process, and those raw materials have significant impacts on the global economy.

In obedience to the early findings, the mechanical properties of alloy materials can be optimized based on the desired response by altering parameters during the process (including hatch style differentiating, contour variations, base plate heating, and internal heat treatment) that has an impact on the final morphology of the printed parts [61]. Ardila, et al. [62] investigated the effect of INC718 recycled powder on the mechanical property using SLM process. The powder had been recycled using a self-developed recycling method, and their findings showed that the mechanical properties of the printed part had not been altered significantly after being recycled up to fourteen times. Moreover, the research shows a possible option to utilize powders that may potentially be recycled several times. This process can minimize raw material consumption and contributes to a better environment. Besides, the powder material thermodynamic phase transformation also significantly impacts the printed part mechanical property [63]. In similar studies, Mazur, et al. [64], Fleißner-Rieger, et al. [65], Martin, et al. [66] have used Thermo-Calc computational thermodynamics software to simulate and control the sequential steps of a phase transformation of the powder material from the temperature of the liquid to an approximate solidus temperature solidification path varying compositions and equilibrium phase composition.

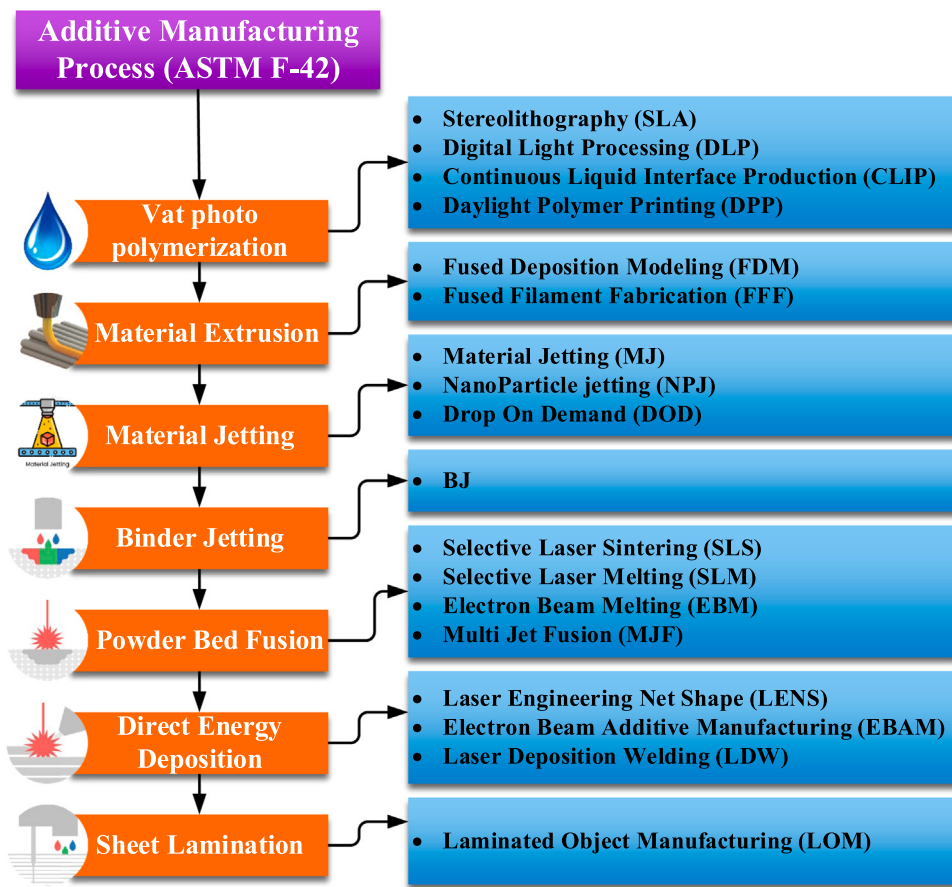


Fig. 2. Classification of Additive Manufacturing process (ASTM F-42) [22,23].

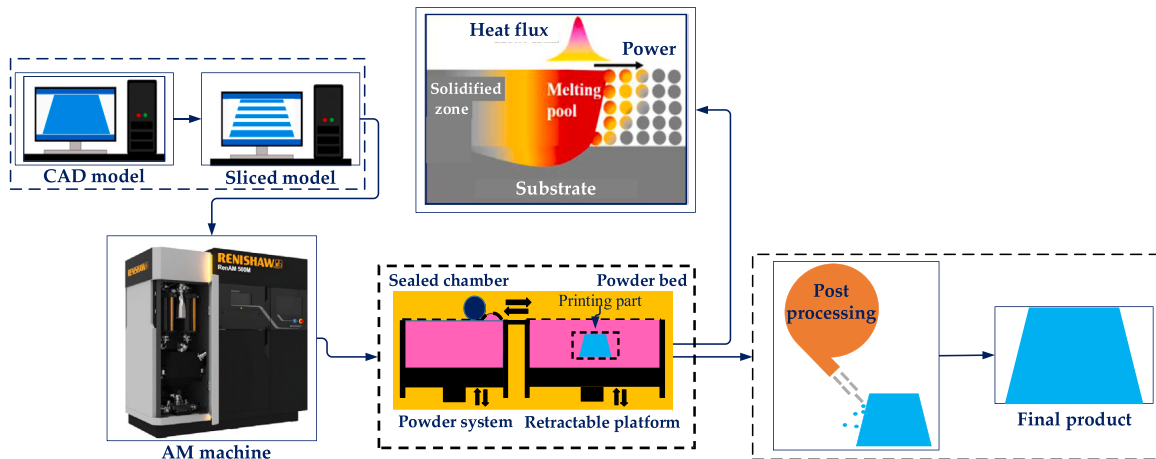
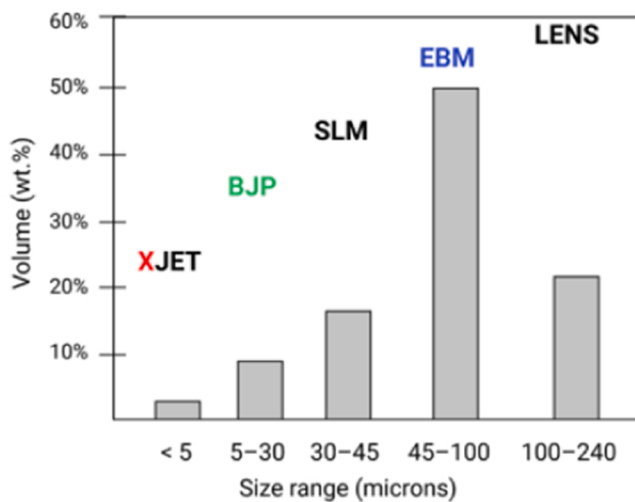


Fig. 3. Working principle of SLM process [44,45].

## 2.1. Printing of smart materials

A shape memory (smart) material is when a thermal or mechanical force is applied to the metallic or polymeric materials to regain their primary shape (designed shape) following deformation (under temperature or stress conditions). However, these materials have poor machinability characteristics in traditional manufacturing systems [67]. SLM process can alleviate for smart materials with poor machinability characteristics such as Nickel-Titanium or Nitinol (NiTi) shape memory alloy within a smart structure of complex shapes. This material is a well-known shape memory smart material used in various products,

including aerospace, biomedical equipment, and various engineering applications. However, due to excessive tool wear, high cutting force, high hardness, and surface defects, NiTi alloys are complex to machine in a conventional process [68–70]. Khoo, et al. [71] studied a new scanning strategy for fabricating NiTi materials using a repetitive scanning strategy method. The laser power used during the first and second scans was 25 and 60 W, respectively, with the laser scanning speed, remained unchanged at 3600 mm/s. The results revealed that variations in the laser absorptivity and heat conductivity of materials before and after the initial scan significantly impacted the fabricated NiTi parts. This repetitive scanning method imparts excellent properties



**Fig. 4.** Crucial powder size range in Additive Manufacturing [46]. XJET: Nano Particle Jetting Printer, BJP: Binder Jet Processing, SLM: Selective Laser Melting, EBM: Electron Beam Melting, LENS: Laser Engineered Net Shaping.

for the printed samples and successfully prints the NiTi materials without defects. A similar study Wang, et al. [72] investigated the phase transformation behavior of NiTi materials using the SLM process. Variable parameters of laser power, scanning speed, hatching distance, and constant layer thickness were used. They obtained that the martensite temperatures changed concerning the scanning speed hatching and laser power parameters. Moreover, the scanning speed with a combination of laser power is a significant parameter for influencing the NiTi ratio and the martensite transformation temperatures of the material. Xiong, et al. [73] investigated the tensile properties of NiTi alloy material using the SLM technique. They utilized an intraformational and laser scanning technique with a stripe rotational scanning strategy. They got minor defects and a significant shape memory effect, with 99% shape recovery after 50% compressive deformation when heated. Taheri Andani, et al. [68] studied the mechanical properties of NiTi materials using the SLM method. They utilized simple cubic, Body Center Cubic, and Body Center Cubic-Z as unit cell geometries. A practical shape memory effect and functional stability were observed on dense and porous printed samples. In addition, the researchers confirmed, porous NiTi structures are also appealing materials for lightweight edifices, energy absorbers, and biomedical implants since they have lower elastic modulus and density than dense NiTi structures while still having good shape memory properties.

## 2.2. Printing of multi-materials

Printing of multi-material parts in the SLM process requires a customized SLM machine that provides two or more powders at a time or sequential. Chen, et al. [74] researchers investigated the influence of process parameters on developing interfacial layers and mechanical characteristics of SS316L and CuSn10 materials using a self-built multi-material SLM machine. The machine has a multiple powder delivery system, see Fig. 6 which consists of two powder feeding devices that feed powders from the outside to the inside of the build chamber. These two inner powder hoppers are connected to the laying car, which can load two different types of metal powder simultaneously, and each powder hopper includes a switch to regulate powder loading and unloading. Moreover, they had been utilized different parameters for both materials, and the result revealed that the interfacial point of the two materials had imparted the maximum mechanical property. In the same study, Demir and Previtali [75] are investigated the mechanical properties of pure Fe and Al-12Si materials using a multi-material SLM machine. The machine has comprised of two vertical powder hoppers, and

**Table 1**

Impact of powder particle size on powder properties from previous literature.

Ref.	Material	Particle size ( $\mu\text{m}$ )	Objective of the study
[48]	SS316L	141.4 84.5	Particle shape, powder flowability, and powder layer density impact the PBF process, focusing on the final part density.
[49]	SS316L	$D_{10} = 4, 13.6, 21.9, 31.2, 37.8, 50.5$ $D_{50} = 9.5, 20.2, 28.3, 37.9, 46.7, 59.3$ $D_{90} = 19.3, 29.7, 35.8, 47.3, 57.3, 71.9$ $D_{90}-D_{10} = 15.2, 16.1, 13.8, 16.1, 19.5, 21.4$	Effect of powder layer density variations in the L-PBF process on the size of particles of monomodal 316 L powder.
[50]	AlSi12 Alloy	$D_{10} = 24, 17, 22$ $D_{50} = 48, 42, 60$ $D_{90} = 71, 85, 94$	Effect of powder properties on AlSi12 alloy in the SLM process.
[51]	AISI 321	0–20 0–40 20–40	Impact of the powder particle size distribution on the structure and characteristics of monolithic AISI 321 using the L-PBF process.
[52]	Inconel 625	$D_{10} = 20, 5, 23$ $D_{50} = 33, 6, 33$ $D_{90} = 55, 9, 48$	Powder properties impacted the microstructure and mechanical behavior of Inconel 625 produced using SLM.
[53]	SS316L	$D_{10} = 7.12, 19.84, 15.26$ $D_{50} = 15.12, 28.26, 37.70$ $D_{90} = 24.17, 41.13, 55.54$	Surface quality and mechanical characteristics of SS316L components are influenced by particle size distribution using the SLM process.
[54]	Pure Tungsten	0 10 20 30 40 50	Particle size effects on laser absorption and scanning track formation in pure tungsten powder using the SLM process.
[55]	SS316L	$D_{10} = 18.49$ $D_{50} = 31.90$ $D_{90} = 48.10$	Powder layer density evaluation of SS316L material using the SLM process.
[56]	AlSi10Mg	$D_{10} = 32, 19, 19, 28$ $D_{50} = 45, 31, 37, 41$ $D_{90} = 63, 46, 61, 61$	To better understand the impact of powder characteristics on the final components produced by metal L-PBF processes under consistent parameter settings, except hatch scanning speed.
[57]	Ti-6Al-4 V	< 25 25–45 45–75 75–106 106–150 150–250 > 250	Identify and control a novel titanium powder precursor for additive manufacturing.
[58]	AlSi7Mg	$D_{10} = 48, 54, 14$ $D_{50} = 63, 70, 31$ $D_{90} = 83, 91, 58$	Compare the powder characteristics of several AlSi7Mg powders produced using different techniques.
[59]	SS316L	Single-mode $D_{50} = 36.31$ Bimodal $D_{50,L} = 36.31$	Bimodal particle size distribution in SS316L using the SLM process.
[60]		$D_{10} = 27.2$ $D_{50} = 50.0$ $D_{90} = 84.9$	Studied microstructure and mechanical properties of a Nitinol-based shape memory material using the SLM process.

the powders are mixed at the third hopper (beneath the two hoppers see Fig. 6) by a vibrating plate. Different parameters are utilized for both materials, and they were obtained from the finding that large cracks have occurred on the printed part interfacial point due to the materials' poor thermo-mechanical compatibility and miscibility. Wei, et al. [76] another study, fabricated the samples using three different types of materials, namely SS316L, INC718, Cu10Sn materials, by a specially

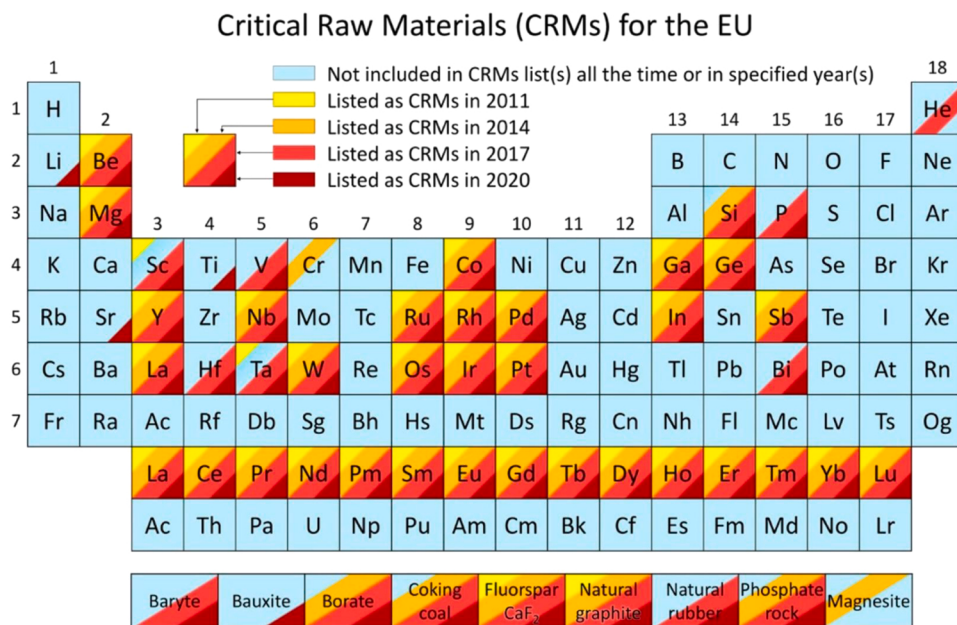


Fig. 5. Critical raw materials list from 2011 to 2020 [46].

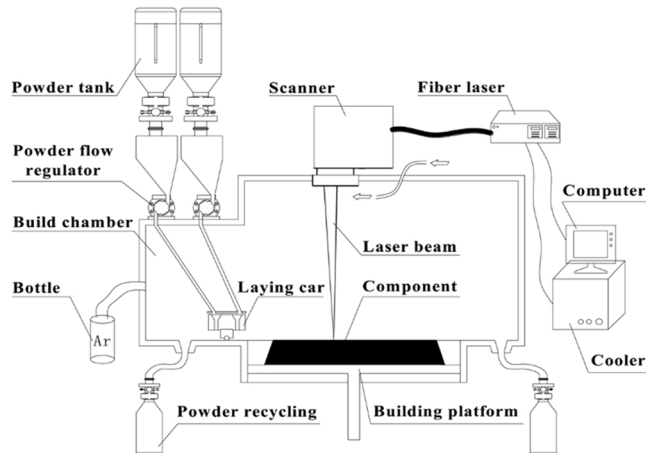


Fig. 6. Multi-material SLM machine [74].

designed multi-material SLM machine. The machine has comprised multiple powder dispensers and traditional roller-assisted powder delivery systems depicted in Fig. 8. The main powder bed delivers SS316L materials to the build plate, and INC718 and Cu10Sn materials are selectively deposited from the dispenser point to point. The result indicates that printing of a combination of materials imparts an excellent mechanical property. However, it needs parameter optimization to reduce defects that occur due to material incompatibilities. In a similar study Wei, et al. [77] has used the SLM technique to manufacture 316 L and Cu10Sn materials using Functionally Grade components in the same and distinct layers. The part was made using a self-developed ultrasonic powder feeder combined with the SLM system, as described in Fig. 8. They observed some unmelted 316 L solid spherical particles entrenched in the fully melted copper alloy region due to the low laser energy density, which was insufficient to melt the 316 L steel materials. Moreover, the higher hardness was obtained from fabricating by 316 L and Cu10Sn material compared to the conventional process. The authors recommended that associated characteristics for each transition material and the combined Functional Grade Material (FGM) mechanical properties should be further studied. Sing, et al. [78] has studied the

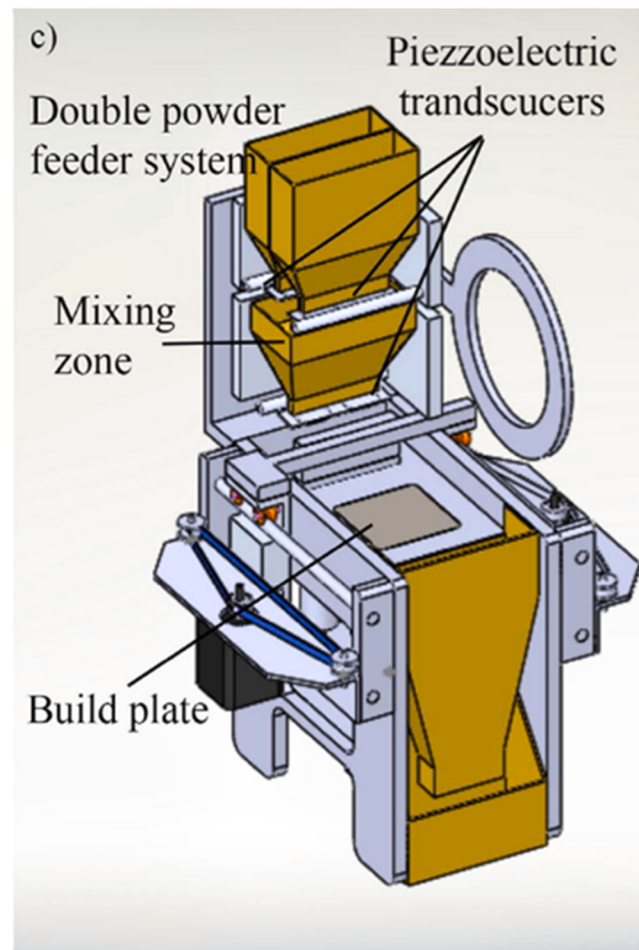


Fig. 7. Schematic diagram of Multi-material SLM machine [75].

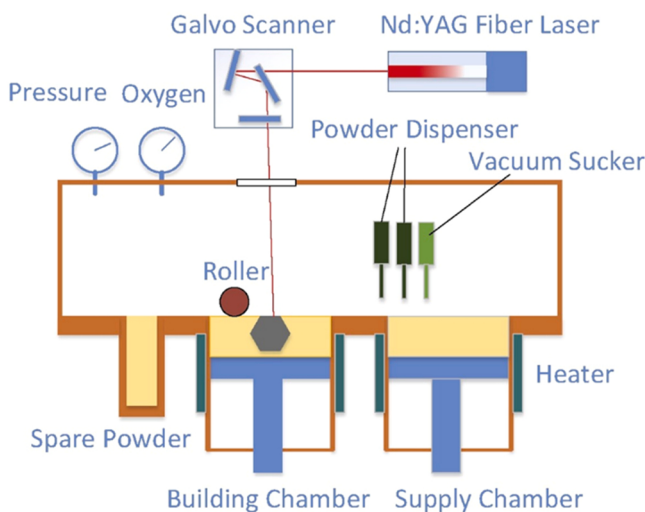


Fig. 8. Multi-material SLM system [76].

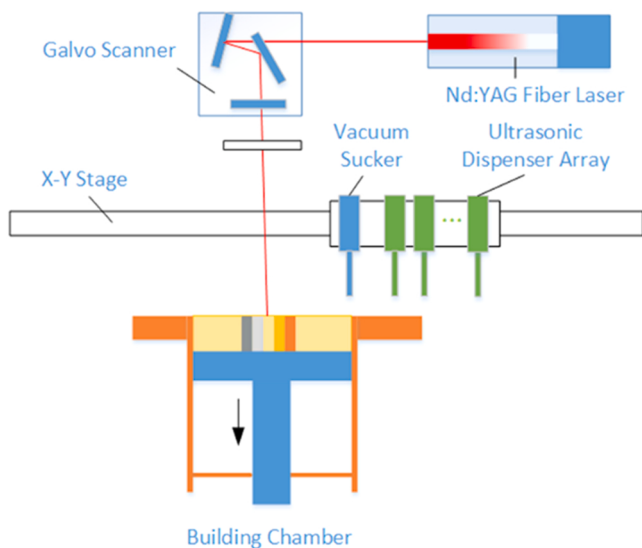


Fig. 9. Experimental setup of Multi-material SLM system [77].

mechanical properties of AlSi10Mg and UNS C18400 copper multi-materials illustrated in Fig. 10 printed in the SLM method. The powder feeding mechanism of the machine has the hopper integrated on

a specifically developed separator in the re-coater, allowing for the storage and selective deposit of two or more materials in each layer. Some changes were made to the recoating program and the CAD file to set the process parameters independently. Their findings revealed that the AlSi10Mg/C18400 contact had a higher metallurgical bonding, and also, the tensile strength of the bimetallic Al/Cu laminates was higher than copper yet lower than AlSi10Mg. Costa, et al. [79] used SLM and Hotpress processing for studied the tribological characteristics of Nickel-Titanium (NiTi) mono-materials of cellular structures with different open-cell sizes and wall thicknesses. To obtain the multi-material parts, they utilized the HotPressing method to introduce the PEEK into the open cells of NiTi structures demonstrated in Fig. 11. The morphological analysis result revealed that the SLM process parameters were suitable for producing high-quality components with empty defects. As contrasted to mono-material NiTi parts, tribological characterization revealed that the multi-material specimens had stiffness and better wear resistance. Hence, to obtain an excellent thermo-mechanical property of the printed part, multi-materials are the best option; however, it needs a customized SLM machine and appropriate process parameters. One more critical thing regarding printing of multi-materials in the SLM process is that the printed material thermo-mechanical property does not have large differences.

### 2.3. Reflective materials

One of the challenges in the SLM processes is printing reflective or precious materials within a complete density due to the poor ability to absorb laser radiation. The laser radiation absorbance characteristic of a material is one of the most crucial properties for printing reflective materials. Wavelengths and temperature also have a significant impact on absorption characteristics. The laser absorptivity of a material is strongly reliant on the irradiated and the laser wavelength [80,81]. When a laser beam hits the powder layers in the L-PBF process, three physical phenomena occur reflection (R), absorption (A), and transmission (T); see Eq. (1). The following is the correlation between the three values based on the ray propagation mechanism: for a further study of laser absorption, refer to [54].

$$R + A + T = 1 \quad (1)$$

When the laser beam hits a substance, the radiation returns, and the other is retained on the specimen. Due to this reason, shown in Fig. 12, the material having a low melting point (Silver, Copper, and other) reflective materials required a high-power laser energy source than the material having a higher melting point [82]. It is challenging to fabricate copper and its alloy using the powder bed fusion process because of its optical absorption and high thermal conductivity [83]. Lindström, et al. [84] have fabricated copper materials coated with a thin Tin and Nickel

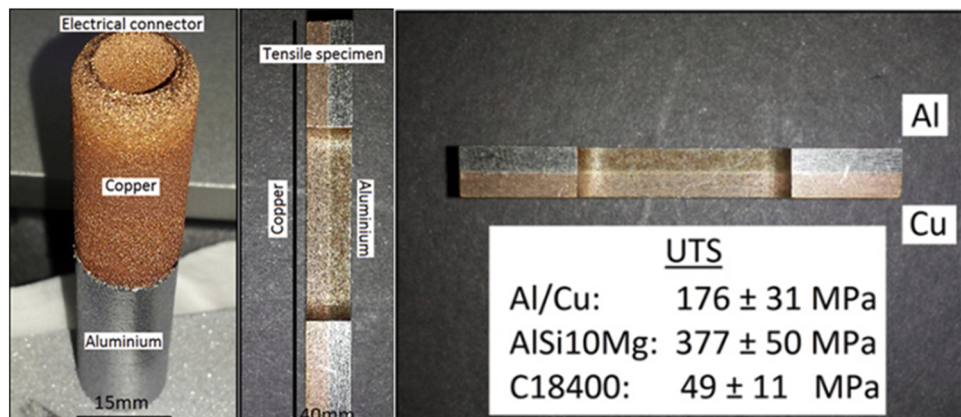
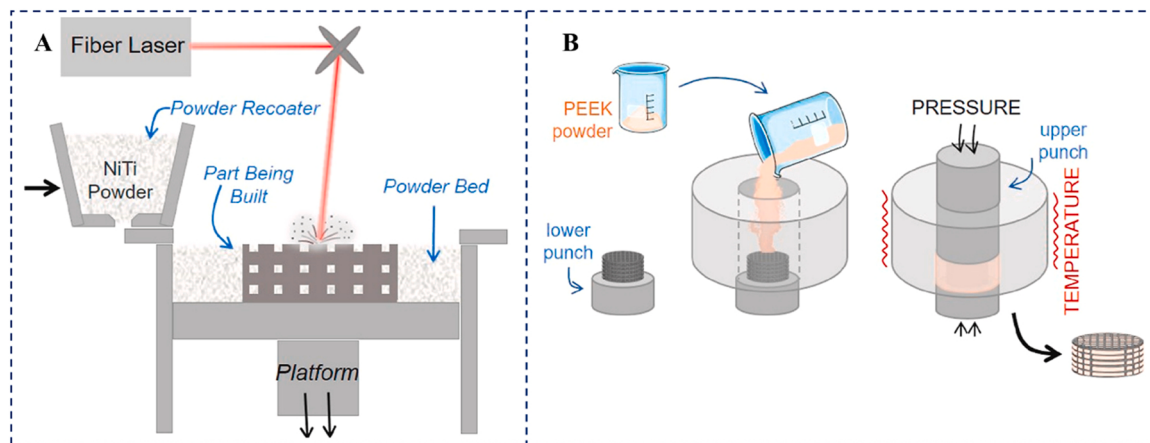
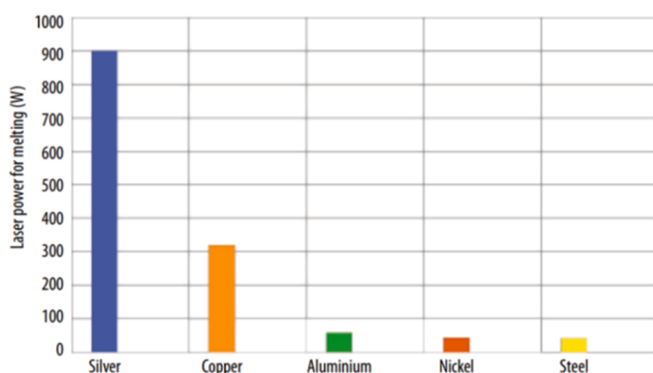


Fig. 10. Multi-material electrical connector and Dog-bone sample [78].



**Fig. 11.** Experimental setup of multi-material printing process: (A) SLM process and (B) Peek impregnation process [79].



**Fig. 12.** Amount of laser power for melting reflective materials [82].

material layer using an immersion deposition method in the SLM process. The porosity of the tin-coated copper specimens was substantially smaller than that of powder mixes of comparable composition. Besides, Nickel-coated powders produce components with a density equivalent to tin-coated powders. Moreover, the reduced porosity is connected to the switch from throwing to conduction welding due to the powder bed's increased optical absorption. A similar study Hess, et al. [85], Prasad, et al. [86] succeeded at depositing and welding copper materials onto copper, aluminum, steel, and titanium substrates through the laser metal deposition process. They conclude that green laser sources have a higher absorptivity than more widely accessible infrared lasers, making them better for copper processing. Jadhav, et al. [87] has proposed using L-PBF to make a fully dense CuSn0.3 alloy coated with tin. Immersion plating methods were used to apply the coated material layer ( $62 \pm 14$  nm) to the surface of the CuSn0.3 alloy. They achieved fully dense and crack-free copper components with excellent thermo-mechanical properties.

### 3. Process parameters

Numerous physical phenomena are involved in the SLM process, including laser absorption and reflection, heat transfers, fluid flow, vaporization, material emission, and chemical reactions. Phase transformations of powder-to-liquid and liquid-to-solid occur at the same time. Understanding these physical phenomena can help fabricate defect-free components effectively and select appropriate process parameters for the SLM process [89]. Under-heating and overheating melting processes on overhang structures or unsteadily melting parts are the most common causes of defects in the SLM process, as illustrated in Fig. 12 [88]. The printed part's quality and mechanical properties can be

enhanced by monitoring process parameters in the SLM process [90] and utilizing various parameters from different scholars are summarized in Table 2. Most of the laser machine parameters illustrated in Fig. 14 impact the buildup and the final phase over the relative density of the component [91]. Modifying specific parameters based on the material property achieves low residual stress, distortion, and excellent printed quality components [92]. Controlling process parameters are the best alternative for getting the desired geometries, mechanical properties, and microstructures. All the responses of the SLM process are susceptible to each process parameter, and it becomes challenging to determine the parameter level magnitude. However, the volumetric energy density equations control the parameter magnitude ranges, not exact points [93–96].

"Volumetric Energy density (VED)" is a critical manufacturing characteristic for melting powder materials. This parameter reflects the laser beam's energy transmitted to a volumetric unit of powder material and correlates with several relevant laser and scan parameters [99]. Moreover, VED is typically composed of four process parameters that are independently controlled: (1) laser power (W); is the energy intensity of the laser beam; (2) scanning speed (mm/s); traverse speed of the laser beam; (3) hatch distance (mm); the gap between two head-to-head scan pathways; and (4) layer thickness (mm); the thickness of a layer that equals one incremental amount of the powder bed in shown in Fig. 15 [100]. An identical energy density value with different SLM process parameters results in different material properties. In addition, the value of energy density differs from material to material, and the value greater than the materials specific energy density range leads to a wider and deeper melt pool [101,102]. The empirical formula of VED was calculated using Eq. (2) [103,104].

$$VED = \frac{P}{Vs * Dh * t} \quad (2)$$

Where  $VED$  = Volumetric energy density ( $J/mm^3$ ),  $P$  = laser power (W),  $Vs$  = scanning speed ( $mm/sec$ ),  $Dh$  = hatching distance ( $mm$ ), and  $t$  = layer thickness ( $mm$ ). Other studies use laser beam diameter ( $mm$ ) instead of hatch distance. Meanwhile, the hatch distance should be co-ordinated with the laser beam diameter to maintain a specific overlap ratio [100].

The volumetric energy density process parameter with scanning strategies directly impacts the shape, size, temperature, and cooling rates within and near the melt pool. Furthermore, the depicted process parameters significantly impact the residual stress and distortion of the printed part. Levkulich, et al. [92] studied the effect of process parameters on the residual stress of Ti-6Al-4 V material using the SLM process and their findings show that raising the layer thickness of the printed part decreases the residual stress and distortion of the material since it increased the energy density. Bang, et al. [31] investigated the effect of

**Table 2**

Parameters used by different researchers for optimizing the SLM process.

Ref.	SLM System	Laser Power (W)	Scanning speed (mm/s)	Layer thickness (μm)	Hatch distance (μm)	Scanning strategy (Type)	Material (Type)
[43]	ProX200 L-PBF machine	164, 191, 218, 246, 273	500, 1000, 1500, 2000	30	60, 70, 75, 85, 100, 115, 125, 135, 180	Hexagonal Island	AlSi12
[47]	EOS M290	300, 335, 370	800, 1050, 1300	30	150, 190	Stripe	AlSi10Mg
[116]	Aeroswift SLM	150, 200, 250, 300,	800, 1000, 1200, 1400	50	80	S-shaped Orthogonal	Ti6Al4V
[139]	MetalSys150	80, 100, 120, 140, 150, 160, 170, 180	800, 1000, 1200, 1400, 1600, 1800, 2000, 2500	20, 40, 60, 80	30, 40, 50, 60, 70, 80, 90, 100	Meander	Ti-6Al-4 V
[140]	Reinshaw AM 250	400	1000	50	160	Stripe	Ti-6Al-4 V
[141]	SLM system (YLM-300)	170, 180, 190	700, 800, 900, 1000, 1100	20	60, 70, 80, 90, 100	skin-core & triple contour	Ti6Al4V
[142]	Farsoon 271 m SLM System	240, 320, 400	600, 800, 1000	30	90, 120, 150	Rotating strip	Nickel based super alloy
[143]	SLM System	99.5, 120, 150, 180, 200.45	397.73, 500, 650, 800, 902.27	30	59.77, 70, 85, 100, 110.23	S-cross	AlSiMg0.75 alloy
[144]	EOS M280	170, 220, 270, 320, 370	500, 600, 700, 800, 1000, 1200	40	80, 100, 120	Bidirectional sweeping	INC718
[145]	MetalSys 150	80, 100, 120, 140, 150, 160, 170, 180	800, 100, 1200, 1400, 1600, 1800, 2000, 2500	20, 40, 60, 80	30, 40, 50, 60, 70, 80, 90, 100	Meander	Ti-6Al-4 V
[146]	TruPrint 1000 metal	175	800, 1000, 1200, 1400	20	200	Chessboard	AlSi10Mg
[147]	SLM 125HL	200, 300	300, 500	50	120, 160	Island	SS304
[148]	EOSINT M280	150, 200, 250, 300	400, 600, 800, 1000	40	120	Stripe	H13
[149]	3D Systems ProX DMP	120, 160, 200, 240	500, 600, 700, 800	30	50, 75	Bidirectional and meander	SS316L
[150]	EOS M290	250, 300, 325, 350	400, 600, 800, 1000	20, 30	70	Rot-scan	Pure Mo
[151]	EOS M290	300, 350, 370	800, 1000, 1200, 1600	30	100	Rotating strip	Al-v-Mg-Sc-Zr alloy
[152]	EOSINT M280	285	960	40	100	Bidirectional without and with rotation	INC718
[153]	SISMA MYSINT100	70, 90, 110, 130, 150	500, 700, 900, 1100	20, 30	40, 60, 80	Chessboard (3 × 3 mm)	Co-28Cr-6Mo
[154]	SLM 125 HL	200, 210, 250	800	30	120	Zigzag	SS316L
[155]	SLM HL 250	180	600	30	90	Island	INC718
[156]	3D Systems ProX 200	150, 250	495, 825	30	60, 75, 85, 105, 115, 120, 140, 150, 155	Bidirectional	NiNb5
[157]	LSNF-1 (Self developed)	200	100, 150, 200, 250	30	50, 100, 150, 200	Unidirectional	AlCu5MnCdVA
[158]	EOSINT M280 SLM	200, 245, 290, 335, 370	200, 250, 300, 350, 400, 500, 600, 700, 800	30, 40	50, 80, 100, 120, 150	Zigzag	Copper
[159]	EOS M290	220.1	775.5	40	110	Bidirectional	17–4 PH
[160]	SLM 280 HL	200, 250, 300, 350	150, 200, 250, 300	30	75, 90, 105, 120	Meander	90 W-7Ni-3Fe
[161]	SLM-YZ250	200	1500	40	40, 50, 60, 70, 80	Bidirectional	NiTi
[162]	SLM 125HL	200, 350	100, 200, 300, 400, 600, 800, 1000, 1200, 1400, 1600, 1800	30	130	Stripes	Al-Ni-Ti-Zr alloy
[163]	EOS M400 system	350–450	300–600	40	80	Meander	INC718
[164]	EOSINT M280	200, 250, 300	600, 800, 1000	40	80, 100, 120	Stripe	Invar 36 & SS316L
[165]	3D Systems ProX DMP 320	70, 79, 88, 97, 106	496, 558, 620, 682, 744	30	82	Stripe	Ti6Al4V
[166]	M2 Cusing	400	120, 140, 160, 180	100	250–350	Cross	Ti-6Al-4 V
[167]	Noura-M100	100, 125, 150, 175,	400, 500, 600	30	70, 80, 90, 100	Chessboard & Helical	Ti-6Al-4 V
[168]	SLM System	200	900	30	90	Unidirectional, Bidirectional, Cross, Island	SS15–5PH
[169]	ProX-DMP-200	300	1500, 1800, 2100	30	45	Meander	TC4–5Cu
[170]	SLM 280HL	100, 175, 200, 250, 350	500, 900, 1035, 1140, 1200, 1600	30, 40, 50	50, 80, 105, 130, 150, 170	checkerboard	AlSi10Mg
[171]	SLM 125HL	140	600	30	80, 120, 160, 200	Stripe	Ti-22Al-25 Nb
[172]	SLM LMP100	70	600, 800	25	24.5	Checkerboard	Co-Cr-W-Mo
[173]	EOS M290	50, 100, 150, 200	200, 400, 600, 800	30	80	Bi directional double pass	Ni50\$6Ti49.4
[174]	Concept laser M2	180	1000	25	150	Islands chessboard	INC738LC
[175]	SLM280	150	750	30	100	Zigzag	Ti6Al4V

process parameters on the mechanical and microstructural properties of SS316L material using the SLM process and obtained from the study, strength, and elongation dropped swiftly as the energy density raised. Besides, the fracture surface of the tensile test specimen that brittleness raised as energy density increased because the amount of oxygen increased, and the hardness improved. Liu, et al. [106] has studied the effect of scanning speed on the microstructure and mechanical behavior of SS316L material using the SLM process. As a result, they found that the scanning speed changed the melting pool boundaries, residual pores,

solidification cells, nano-inclusions, and grain size and distributions significantly. The maximum tensile strength of 707 MPa was achieved at the maximum scanning speed of 1000 mm/sec. Xiong, et al. [107] successfully studied the effect of process parameters on silver alloy materials' morphology and mechanical properties using the SLM process. The result showed that laser power of 100 W and scanning speed of 1025 mm/sec are significant parameters and level settings for getting the maximum hardness of 148.9 HV within 96.7% density. Kang, et al. [108] studied the effect of laser power and scanning speed on the

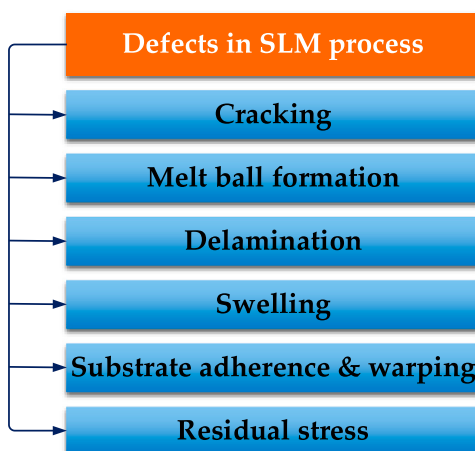


Fig. 13. Common defects in the SLM process [88].

morphology and mechanical properties of INC718 material. The result showed that laser power of 200 W and scanning speed of 1000 mm/sec with a combination of other parameters bestow the maximum tensile strength of 1055 MPa with elongation of 29.5%. In addition, the laser power raises with the reduction of scanning speed, the size of the melt pool increases, less porosity is observed on the microstructure, and the mechanical properties also increase. Miao, et al. [109] studied the effect of scanning strategies on Ti6Al4V materials using the SLM process, and the result indicates that the formation of porosity and surface roughness are delicate to the stripe scanning strategy parameter. Besides, thermal gradients are less marked in the chessboard scanning strategy, and also the number of defects and surface roughness is reduced on the chessboard scanning strategy. Yuan, et al. [110] investigated the effect of laser scanning speed on the different states of the molten pool of SS316L material using the SLM process, and their findings showed that residual porous might be formed, extremely low laser scanning speeds due to keyhole evolution result in a drop in bulk density. Enneti, et al. [111] studied the effect of process parameters on the tungsten material using the SLM process. They obtained a higher density at a low scan speed and hatch spacing. The result shows that density is contrariwise proportional

to hatch spacing and scan speed. Maamoun, et al. [112] investigated the effect of parameters of Al-Alloy materials on the SLM process. They found that utilizing a high laser power value is a significant parameter for increasing the melting rate and energy on the relative density of the built part. Bremen, et al. [113] reported that the hatch distance is determined by the laser beam diameter, which is usually equal to or approximately 0.7 times the beam diameter see equation (3).

$$0.7 \times d \quad (3)$$

Where  $d$  is the laser beam diameter.

In the SLM process, the energy density process parameters such as laser power, scanning speed, hatch distance, and layer thickness are significant to the thermo-mechanical property of the printed parts. All the parameter level settings see Fig. 16 have their significance on the quality criteria of the response study. Furthermore, getting a higher quality product is not easy without combining each VED parameter. For instance, laser power and scanning speeds are the most significant parameters and indistinguishable parameters. If the laser power is raised, the scanning speed must be decreased and vice versa. Both parameters are used to accomplish a complete melting process, getting higher density and a good surface finish. Parameters must be selected based on the response quality criteria, machine specification, type of materials, and interaction of one parameter with the others must be considered. Besides, the characteristics of powder melting are determined by the

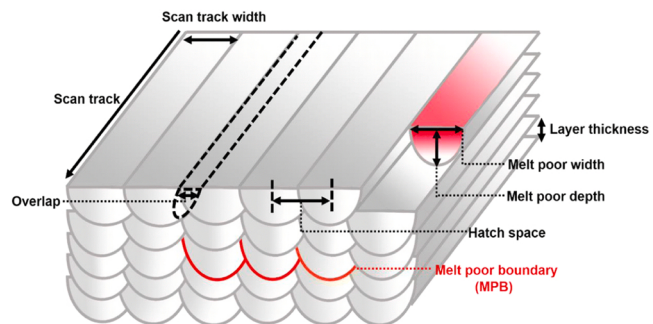


Fig. 15. Graphical representation of SLM process parameters [105].

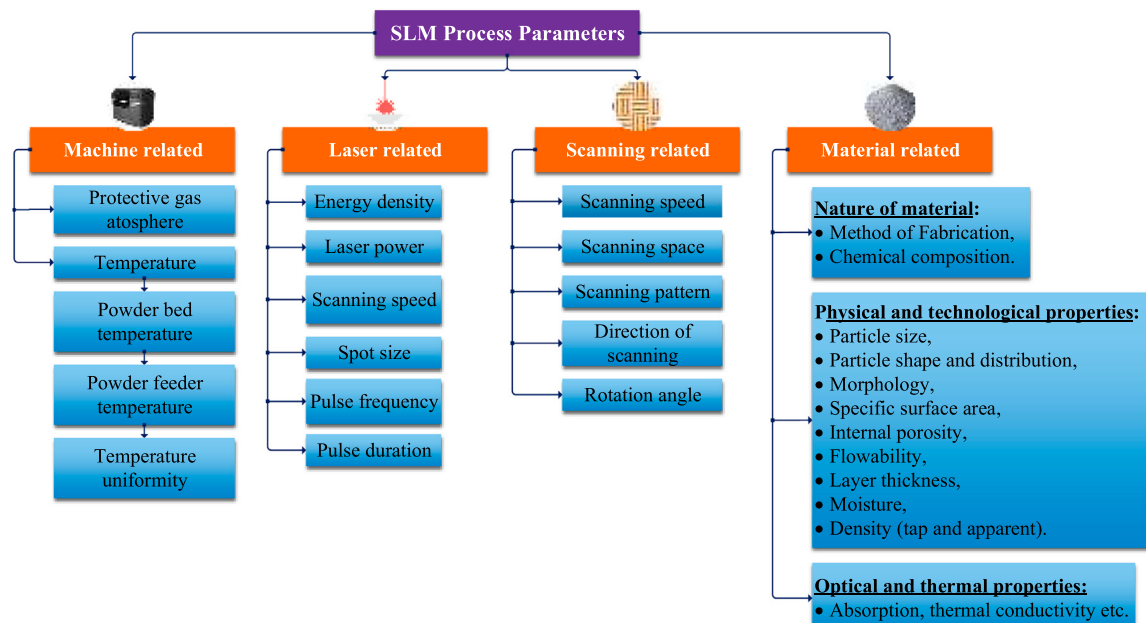


Fig. 14. Major SLM process parameters [93,97,98].



Fig. 16. Effect of SLM process parameters [95, 100, 107, 112, 114–121].

VED equation. One more significant parameter that is excluded in the energy density parameter is a laser scanning strategy. A laser or electron beam movement pattern influences the mechanical properties, microstructure, and induced residual stresses on the printed parts. Most scholars have agreed that the use of shorter scan vector lengths minimizes the residual stresses on the printed part [122]. Varieties of scanning strategy techniques are presented in Fig. 17 to control the printed part's textures and densities. Island (chessboard), unidirectional and bidirectional are the most common scanning strategies in the SLM process. The scanning strategy for a chessboard comprises of dividing the region into tiny cells [123]. Unidirectional scanning is the most basic technique, and it usually results in the least amount of densification and the firmest texture, but other variations have superior densification behavior [124]. The benefit of the bidirectional scanning method is that it is the simplest to create from a CAD file. Low speed causes huge temperature gradients to be consolidated all across the square surface, an unfavorable scenario. However, scanning strategies depend on the type of materials and the required response study of microstructure and mechanical properties [125].

Another study Mercelis and Kruth [128], Zaeh and Branner [129], Kruth, et al. [130] proposed reducing the residual stress of stainless steel alloy and Ti-6Al-4 V material printed by the SLM process. They used the island scanning method and employed various Chessboard block sizes to examine the influence of the Chessboard scanning method on residual stress at the 90° alternating approach, and it was shown to be the most effective in obtaining the lowest residual stress. Wan, et al. [131] investigated the influence of the scanning approach on the mechanical properties of INC718 material using the SLM process. They used two scanning strategies: bidirectional scanning without a 90° rotation between

layers. The findings show that bidirectional scanning without rotation specimens has higher tensile and fatigue strength than bidirectional scanning specimens with a 90° rotation. Also, the process-induced fine grain structures, rather than void size, crystallographic orientation, or dendritic structure, were shown to be the primary cause of the bidirectional scanning without rotation specimen resulting in excellent mechanical characteristics at room temperature. On the other hand, powder melting methods such as single, double, and multiple track (pass) methods are significant on the printed part's mechanical and microstructure properties. When the number of melting cycles is increased, the cooling rate also increases, which improves the microstructure, mechanical property of hardness, and reduces porosity. However, all the track melting methods highly depends on the energy density process parameters Karimi, et al. [132], [133]. Build orientation is another parameter that significantly impacts the mechanical properties of the printed part. For printing the part with a high length-to-height ratio, vertical, inclined, and horizontal build orientations depicted in Fig. 18 are common alternatives. According to the study Rashid, et al. [134], they attempt to quantify the relationship between relative density and building orientation used the new term energy per layer ( $E_l$ ) equations. It can be calculated using Eq. (4).

$$E_l (J) = E (J/mm^3) \times t (mm) \times A_p (mm^2) \quad (4)$$

Where  $E_l$  = energy per layer,  $E$  = energy density supplied,  $t$  = powder layer thickness, and  $A_p$  = printing area per layer. Furthermore, the value of  $E_l$  differs from material to material.

Mfusi, et al. [135] studied the effect of orientations on the mechanical properties of AlSi10Mg material using the SLM process. The samples are printed in the orientation of vertical, horizontal, and inclined styles. Moreover, they obtained different properties in different

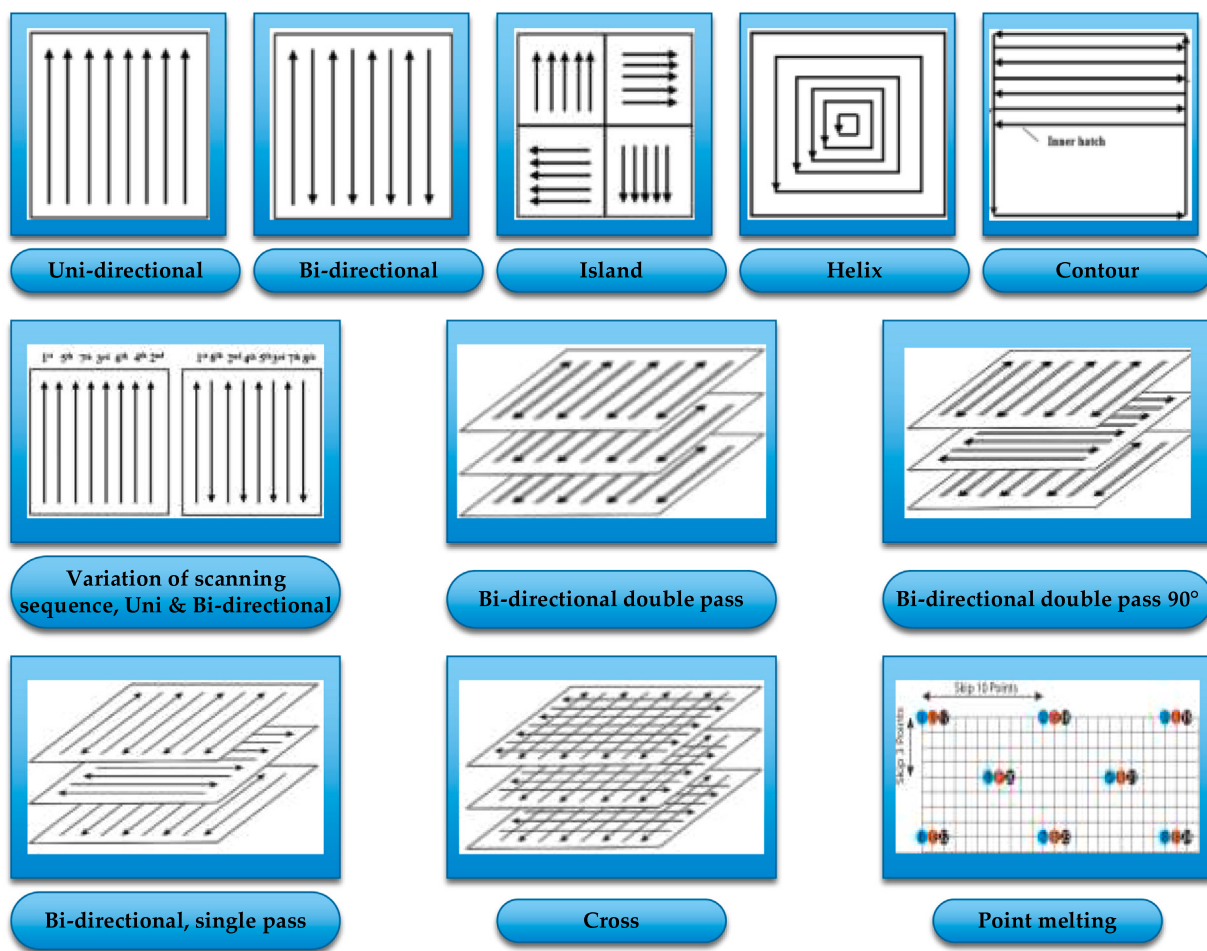


Fig. 17. Common types of scanning strategies [123, 126, 127].

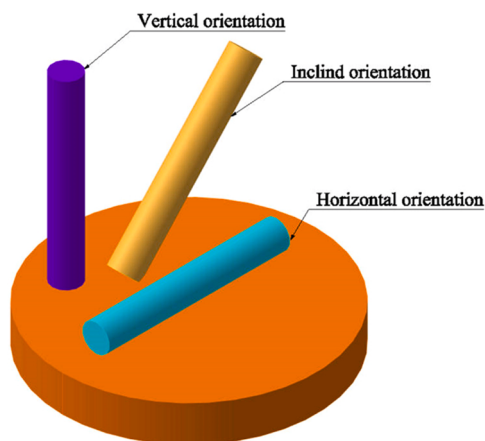


Fig. 18. Orientations on the build plate [134].

build orientations, and the maximum tensile strength was recorded on the horizontal orientations. Simonelli, et al. [136] investigated the influence of build orientations on the mechanical properties of Ti-6Al-4 V alloy using SLM process. Dog bone samples are printed in three different orientations: vertical, horizontal flat, and horizontal edge directions. The results revealed that the material's ductility, particularly its tensile strength, strongly relies on its build orientation. In a similar study, Hartunian and Eshraghi [137] used three distinct built orientations of vertical, horizontal flat, and horizontal edge directions, and they

obtained different tensile strength and brittle fracture features on the materials. Shunmugavel, et al. [138] studied the effect of build orientations on the machinability of Ti-6Al-4 V alloy fabricated using the SLM method has been investigated. The samples are machined using orthogonal cutting techniques. The findings revealed that build orientation substantially impacts the chip formation of parts produced using the SLM method. Due to the sticking phenomena and strong friction that occurs between the tool-chip surfaces, the longest continuous chips are obtained in the vertical and horizontal directions. Generally, build orientation plays a significant role in the mechanical and microstructure of the material.

#### 4. Printing of lattice structure in SLM process

Cellular materials such as foams, honeycombs, lattices, and similar structures illustrated in Fig. 19, are an appealing alternative for many design applications, particularly light-weight design, due to their porous structures, high specific strength, and stiffness properties [176,177]. Lattice structures are cellular structures fabricated in 2.5D or 3D geometries using several methods: investment casting, a hybrid of extrusion and electro-discharge machining, composite fabrication methods, including textile weaving [178], and additive manufacturing process [179]. Fabricating lattice structure with AM process allows to manipulate the unit cell strut thicknesses, shape, and a combination of material usage alternatives compared to the conventional manufacturing processes [180]. The structure has suitable for a wide range of industrial applications (aerospace, biological engineering, mechanical engineering, and so on [181]. Considering numerous inherent applications and

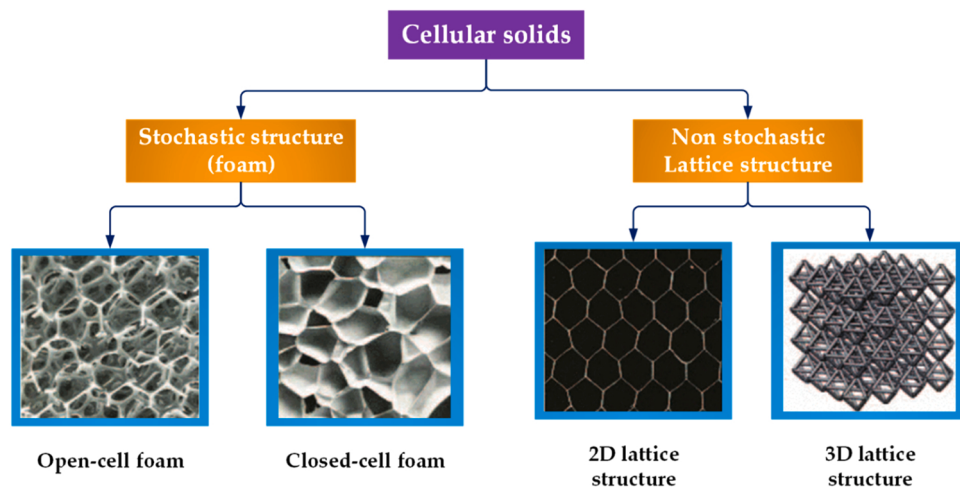


Fig. 19. Classification of cellular solids [180].

benefits of the lattice structure printed by the SLM process, it has higher specific strength and piqued attention. Many different lattice structures have been conceived and printed in this process using the most popular materials to print lattice structures in the SLM process such as Ti-6Al-4 V, SS316L, CoCr, Al-Si alloys, and Ni alloys [182,183]. For printing lattice structures in the SLM process, choosing the appropriate process parameters is crucial. Several parameters influence the quality of SLM printed part, including powder shape, size, and chemical composition, particle size distribution, laser exposure strategy and power, scan speed, layer thickness, and hatch distance. Those parameters and their level settings have various effects on the mechanical properties of the lattice structures [178, 184–186]. In this process, printing lattice structures has some limitations, i.e., beneath the overhanging surfaces, the part cannot be printed without enough geometric distortions. This minimal slant angle is determined by process parameters, type of material, and powder properties [187,188]. [189] using the SLM process, investigated the elastic and failure responses of a 3D octet and rhombicuboctahedron unit cell lattice structure. Furthermore, they recommend that the failure causes of SLM lattice structures should not

be restricted to cell topology and geometry. However, geometric defects caused by SLM, such as strut waviness, strut thickness fluctuation, and strut oversizing, play a significant role in SLM lattice structure failure. Ravari, et al. [190] the impacts of geometry, microstructural defects, and asymmetric material responses of dense shape memory alloys are investigated on the mechanical response of cellular structures. Their results revealed that the performance of lattice structures is further hindered by microstructural flaws coming from the SLM process. In this process, the printed part defects are minimized using appropriate process parameters (different process parameters for different lattice structures used by previous scholars are listed in Table 3). Numerical modeling also plays an excellent role in accurately minimizing defects to print the complex lattice structure parts [191]. Yan, et al. [192] are studied the feasibility and printing performance of SS316L gyroid cellular lattice structures produced by the SLM process. Their findings showed that Gyroid structures with struts positioned at 0 and 90 degrees to the building direction have higher mechanical characteristics than those with struts oriented at 45 degrees. A similar study Amani, et al. [193], [194] revealed that when laser power increases, mechanical

**Table 3**  
Parameters used by different researchers for printing lattice structure in the SLM process.

Ref.	SLM system	Laser Power (W)	Scan speed (mm/s)	Layer thickness ( $\mu\text{m}$ )	Hatch distance ( $\mu\text{m}$ )	Unit cell size (mm)	Lattice type	Materials
[199]	Renishaw AM400 SLM	200	1250	30	100	5	Periodic diamond	AlSi10Mg
[200]	3D Systems ProX-300	170	1600	40	50	2	BCC & Octet-truss structure	17-4PH
[195]	SLM, E-Plus	80–100	570–2100	0.06–0.08	0.02	5	Tetrahexahedron, diamond & BCC	316 L SS
[201]	EOS M290	370	650	30	110	4	Diamond and TPMS	Cu-Cr-Zr
[202]	SLM Solution 250HL	200	900	30	120	2–4	BCC and FCC	Inconel 625
[203]	SLM 250 HL	150	400	30	80	1–2	Cubic and Honeycomb	Ti-6Al-4 V
[204]	EOSINT M280	280	1200	30	120	2–6	Topology optimised	Ti6Al4V
[186]	SLM system	350	921.05	50	190	7.5	BCC and FCC	AlSi12Mg
[205]	SLM250HL	175	710	30	120	2, 3	BCC and FCC	Ti-6Al-4 V
[206]	SLM system	95	250	75	75	2–8	Gyroid	316 L SS
[207]	SLM 500 solution	290	1200	40	120	4	Vertical and Radial gradient	Ti-6Al-4 V
[208]	ProX200 SLM	285	2500	40	100	5	F2BCC (Combination of BCC & FCC)	AlSi-12
[209]	SLM Solutions	150	1000	30	50	0.6–1	BCC	SS316L
[210]	SLM Solutions 500 HL	240	1150	60	105	3–4	BCC & FCC	Ti6Al4V
[211]	EOSINT-M280	370	1500	30	130	10	BCC	AlSi10Mg
[212]	SLM250HL	173–350	710–921.05	30, 50	120, 190	2–7.5	BCC & FCC	Ti6Al4V & AlSi12Mg
[213]	SLM Solutions 125	100	385	30	120	2–3	Gyroid	CP-Ti
[214]	SLM system	150	1750	20	75	1.5	Schwartz	Ti-6Al-4 V
[215]	EOSINT-M270	170	1250	30	60	3–7	Gyroid TPMS & Diamond TPMS	Ti-6Al-4 V
[216]	EOSINT M 270	170	1250	30	100	19.4–36.2	Cube	Ti-6Al-4 V

characteristics improve. Zhong, et al. [195], Sing, et al. [196] are studied the mechanical behavior of SS316L and Titanium-tantalum materials via the SLM process. Their results revealed that increasing the volume fraction, or relative density, improves mechanical characteristics. The mechanical properties of lattice structures are generally represented as a percentage of the mechanical properties of their parent material. They are dependent on the relative density of the lattice structure and mathematically expressed [197] in Eq. (5):

$$\frac{\rho^*}{\rho_s} \quad (5)$$

Where:

$\rho^*$  is the ratio of the apparent density of the cellular structure,  
 $\rho_s$  is the density of the cellular structures of the material.

The lattice structure is also a crucial aspect of the effect of mechanical properties. Bai, et al. [198] are designed and suggested an improved All-Face-Centered Cubic (AFCC) lattice structure with six faces and eight vertices. For evaluating the new design compared with a Body-Centred-Cubic (BCC) lattice structure printed with the same parameter levels via SLM Process. The result revealed that the AFCC lattice arrangement outperformed the BCC structure's mechanical properties while maintaining a low weight. Generally, unit cell structures, materials, and process parameters significantly influence the mechanical and microstructural lattice structures printed by the SLM process.

## 5. Support structures in SLM process

Support structures are crucial in the SLM process, mainly when re-orientation eliminates overhanging features. These structures act as anchors, disperse heat, and prevent thermal expansion distortion [217]. Support structures are required for various reasons in the AM printing processes. Specific applications require such a structure to endure deformation or even implosion induced by gravity as the part is being printed or tethering components that are currently unattached to the main body of the printed part during fabrication. Support structures can also reduce the impacts of temperature gradients during the manufacturing process and shrinkage after solidification, which are common in many AM methods. Various supports are employed in metal AM processes, such as block, point, line supports, see Fig. 20, and those have a unique set of capabilities and applications [218]. Some of the pros of support structures help prevent cracking, curling, sagging, delamination, and shrinking caused by heat deformation [219]. However, the inclusion of support structures increases the part fabrication time, manufacturing cost, and the complexity of post-processing operations. As a result, geometrical design and optimization of support structures are vital to improving the durability and efficiency of the parts produced via SLM. Orienting the object into an ideal printing position is one of the most efficient techniques to diminish the required support. Overhanging sections illustrated in Fig. 21 require support structures or the optimal orientation position [220].

Li, et al. [221] studied a lightweight and support-free (L&S) design technique for printing parts using the SLM process. They used Topology

optimization (TO) to make the components lighter, and a support-free design method was created to allow them to make parts without supporting structures. The results demonstrate that parts designed using the L&S approach do not require post-processing to remove support structures, reducing overall cost and manufacturing time (comprising pre-processing, manufacturing, and post-processing time). However, the case study revealed that the research has one drawback: the redesign process resulted in a 20.8% volume increase, of which 13.6% volume increase belongs to the support-free design approach.

Cooper, et al. [222] have successfully studied contact-free support structures for minimizing it during the printing of parts in the P-PBF process. The gap distance and the support thickness were used to print the part shown in Fig. 22, two novel concepts or parameters important to its function. The gap distance determines the improved heat flow; the smaller the gap distance, however, binding between the head support and the overhang can occur if the gap distance becomes too tiny. On the other hand, the thickness of thermal support can influence its heat dissipation capability; in principle, the thicker is better, however, this results in more incredible material waste. It also showed that the usefulness of heated support depends on the gap distance and the thickness of the heat support. Furthermore, the contactless heat support has been demonstrated to apply to a wide range of overhanging shapes, comprising varied curves and geometries. Another essential consideration is the use of a self-supporting design that eliminates the required support structures. For example, the Gyroid cell type is intended to form periodic lattice structures and uses its curved cell surface as a self-supporting feature, eliminating the requirement for support structures and minimizing material waste and production time [192].

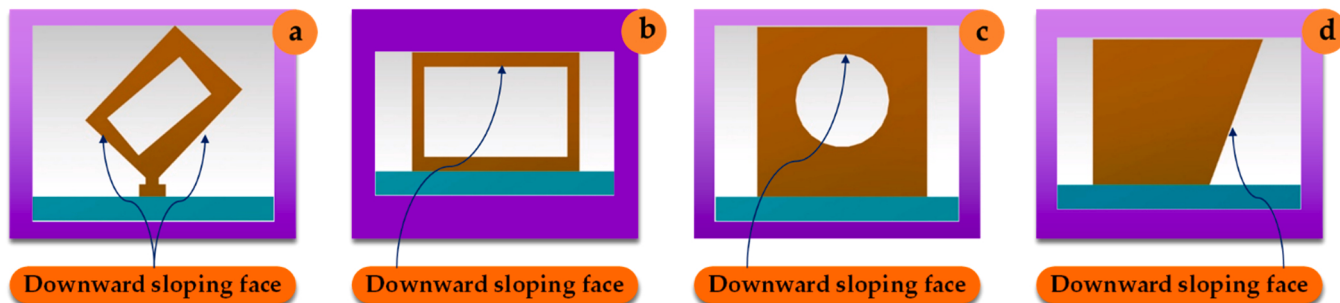
Cao, et al. [223] studied a new approach for enhancing the machinability of cone support structures for parts produced by the SLM process. They used epoxy resin to fill up the openings between the whole cone support components, resulting in solid composite construction. It was found that the epoxy resin had been fully cured. The proposed support removal technique efficiently protects the cone supports from tilting and cave-in during the machining process, enhancing cone support removability. The cutting forces in the x, y, and z axes are reduced instantaneously by the newly discovered approach, and the specific cutting energy is diminished by 22.6%. It is possible to avoid creating cracks, eliminate the spread of process-induced porosity by SLM, and significantly minimize workpiece surface damage. Generally, support structure utilization diminishes the printed part's distortion effect; inversely, it increases manufacturing cost, fabrication time, and post-processing.

## 6. Post-processing

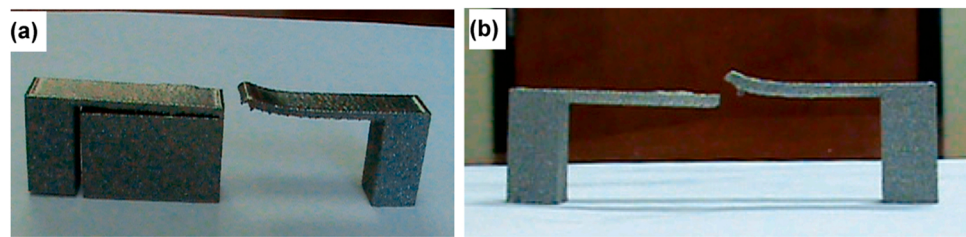
The surface quality of the manufactured component is one of the major challenges in the metal AM process. The process required post-processing to get the desired surface quality. Laser polishing, magnetic field-assisted finishing, grinding, blasting, polishing, and other post-processing techniques, see Fig. 23, have been used with the additive manufactured metallic components to increase surface quality and regulate surface integrity characteristics. Excluding grinding and mechanical polishing, research indicates that the bulk of these procedures



Fig. 20. Different support geometries for metallic parts [218].



**Fig. 21.** Examples of support overhanging structures: (a) downward sloping face, (b) downward sloping face, (c) downward sloping face, and (d) downward sloping faces found by orientation in the building platform [220].



**Fig. 22.** Printing of cantilever overhanging parts: (a) Isometric view, and (b) side view: the left figure is with minimum contact heat support, and the right one is without support [222].

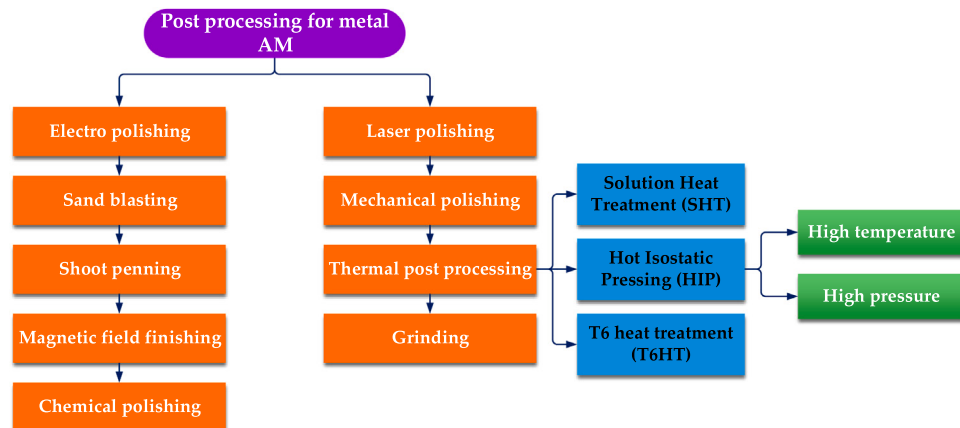


**Fig. 23.** Classification of Metal AM post-processing [225,229].

fail to fulfill the surface criteria [224,225]. Karami, et al. [226] studied a combination of continuous and pulsed laser scanning modes, the parameters above, and their influence on lattice titanium's compressive mechanical characteristics and fatigue behavior. The effects of different post-processing treatments, including Hot Isostatic Pressing (HIP), sandblasting, and chemical etching, were studied on the resultant materials' quasi-static mechanical characteristics and fatigue endurance. The continuous laser approach produced fewer defects and more excellent fatigue resistance. The pulsed laser produced a more homogeneous microstructure, resulting in more isotropic behavior. Furthermore, the bigger previous grains in the continuous mode were specially oriented in the building direction, whereas more refined equiaxed grains with no preferred orientations were seen in pulsed specimens. The maximum degree of fatigue life was achieved using an optimal HIP, sandblasting, and chemical etching mix. Maamoun, et al. [227] has studied the use of recycled powder in the thermal post-processing of AlSi10Mg materials fabricated by the SLM method for improving microstructure uniformity and reducing fabrication costs in the metal AM process of optics and optomechanical systems. To achieve this

objective, a complete characterization of virgin and reused powder and its microstructure evaluation of the fabricated specimens were made. Various process conditions were used to apply annealing, Solution Heat Treatment (SHT), and heat treatment (T6 HT). The results showed that thermal post-processing improved microstructure homogeneity under particular SHT and T6 HT settings. In addition, a micro-hardness map was created to help select the best post-processing parameters to meet the part's design criteria. Zhang, et al. [228] investigated the influence of post-processing on the mechanical behavior of Ti6Al4V materials' fracture toughness and Fatigue Crack Growth (FCG) and the impact of post-SLM thermomechanical treatment and surface machining of the SLM-printed specimen. Ti-6Al-4 V was tested for fracture toughness and FCG in three post-processing states: as-built, heat-treated, and Hot Isostatic Pressed (HIPed). The samples were examined on the built and machined surfaces. Microstructure and fractography were also evaluated to investigate the relationship between the manufacturing process, microstructure, and mechanical properties. Due to the apparent martensitic microstructure and residual stresses, the results show that as-built SLM Ti-6Al-4 V has low ductility and FCG property.

## 7. Simulation software for SLM process

Because of the complication of physical processes during L-PBF, simulations have become essential tools to comprehend the process. In a wide range of engineering fields, Finite Element Analysis (FEA) is one of the most extensively utilized techniques for solving boundary, initial, and eigenvalue issues [230]. Thermomechanical and inherent strain-based approaches are the most extensively applied FEA techniques in the L-PBF process to determine the process-induced distortions. ANSYS Additive Suite (AAS) [231], MSC Simufact Additive [232], ABAQUS AM [233], Autodesk Netfabb [234], and Additive Works Amphion [235] are working on the principle of thermomechanical approach (ANSYS Additive Print AAP, used inherent strain modeling approach). Furthermore, the above-depicted softwares are meant to simulate the SLM process to avoid unexpected machine downtime and enhance the printed part quality by predicting the deformations and stresses from the AM printed parts during the fabrication process.

### 7.1. Ansys additive suite

Ansys Additive Suite (AAS) is a single workbench in the ANSYS software that can predict the residual stresses and deflections using a thermo-mechanical modeling approach. The designed part will first mesh overall using layered voxel (HEX) or tetrahedral (L-TET) mesh type. Later the temperature will be applied in the form of a “Lumped Layered approach.” In this software, laser power and scanning speed need a python script to address its magnitude. Compared to ANSYS Additive Print (AAP) software, AAS is more accurate since it considers the temperature field and the solidified materials real, local thermal strains and comes at a higher level monetary expense. In AAS, considerably more input parameters are required than in AAP. Only basic temperature-based material properties must be defined for process simulations, and no additional calibration is required; basic information of AAS software is depicted in Fig. 24 [236]. Pagac, et al. [232] studied distortion of AISI 316 L materials using experimental and FE analysis methods, and the part was printed via the SLM process. They utilized ANSYS Addictive Suite and MSC Simufact Additive FE tools and obtained a closer result to the experiments from ANSYS Additive Suite software considering deviation values.

### 7.2. Ansys additive print

Ansys Additive Print (AAP) is a standalone and user-oriented software that simulates SLM processes using the inherent strain modeling approach. The simulation is run with a limited number of materials, and those input material properties such as elastic modulus and Poisson ratio, yield strength, bilinear elastic-plastic deformation characteristics, and the AM machine parameters are considered. In this software, the SLM build-up process is simulated by a layer-wise activation of voxel components that all have the same inherent strain at the start. The applied initial inherent strain must be calibrated against the printed geometries. It has an appropriate window for creating optimal support structures and generate distortion-compensated STL files [237]. The assumed strain mode is the most straightforward alternative option, making it ideal for initial understanding. However, the scan pattern and thermal strain modes take much more extended processing, and more data processing results in more accurate predictions. Linear elastic and elastoplastic stress modes have similar trade-offs (i.e., simulation accuracy and solving time). The simulation part should be aligned in the required printing direction (Z-axis) and translated into a stereolithography (STL) file on the geometrical side. The voxelization approach is used to mesh the data [238]. The calibration process depends on materials, machine parameters (laser power, scan speed, layer thickness, baseplate temperature, hatch spacing, slicing stripe width, and scan pattern), simulation type performed (Assumed Strain, Scan Pattern, or Thermal Strain), and stress mode selected (linear elastic or J2 plasticity). Thereby inherently comprises information on the machine specification, AM process parameter, and the type of powder material specification.[231]. Basic information of the AAS software is illustrated in Fig. 24.

### 7.3. MSC Simufact additive

MSC Simufact Additive software is developed for L-PBF and DED processes, specifically to the powder bed fusion to analyze the process [232]. The software has three modules: mechanical, thermal, and thermomechanical workbenches, to analyze the deformations [235]. One of the distinct benefits of this software is the ability to simulate the entire AM process, comprising printing simulation, support cutting, heat treatment, Hot Isostatic Pressing (HIP), analysis of residual stresses and

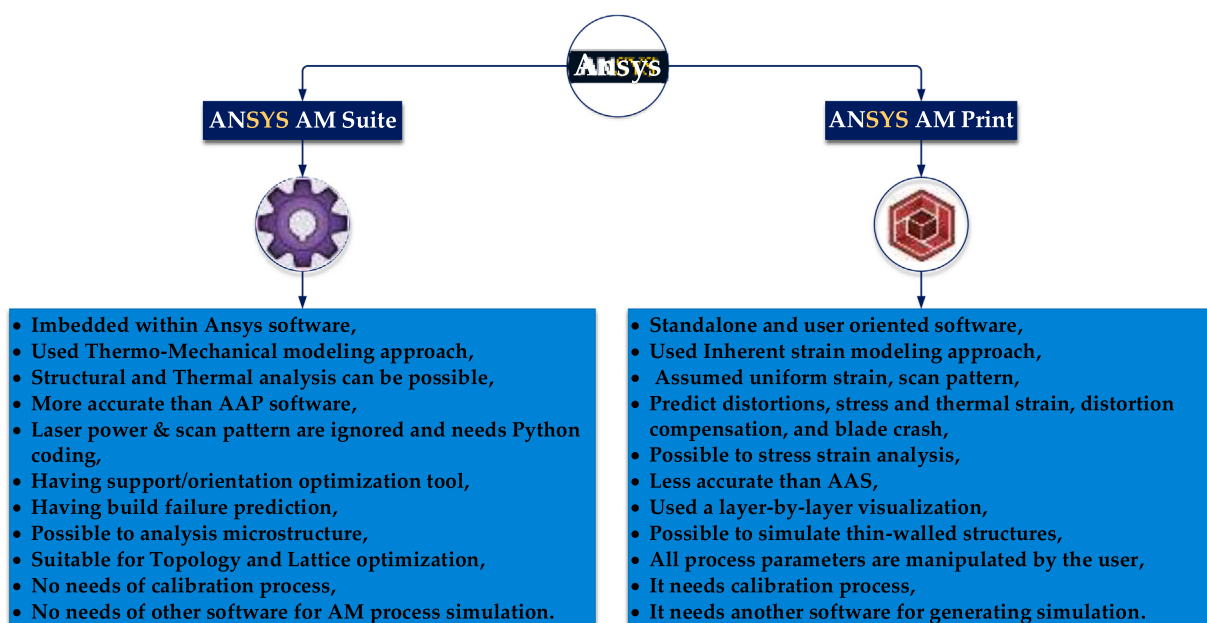


Fig. 24. Comparison of Ansys Additive suit and Ansys Additive Print [231, 232, 236–238, 242].

distortions, detect local hot spots, automatically determine the optimal build orientation and optimize support structures, potential manufacturing issues and examination of microstructures. It also compensates for distortion by defining permissible deviations and producing geometry with the minor deformation [237] and by only utilizing a hexahedral voxel element to discretize the number of elements [239, 240]. The working flow steps and their applications are mentioned in Fig. 25. Huo, et al. [241] investigated different parameters' influence on the distortion and residual stress of INC718 materials fabricated by the SLM process. They employed four different parameters with five-level magnitudes according to L<sub>25</sub> orthogonal array methods. The result indicated that the simulation result obtained from Simufact Additive is much closer than the experimental results from the optimal parameter settings.

#### 7.4. ABAQUS

ABAQUS AM plug-in workbench is embedded in the ABAQUS software that uses a thermomechanical coupled analysis model to predict residual stress and deflection [233]. In this software, the heat input of the scanning laser is represented by a Gaussian distributed moving heat flux. The heat flux is applied on the powder layer's top surface by defining the FORTRAN-based subroutine DFLUX program [243]. Woo, et al. [244] has developed the DFLUX subroutine code in ABAQUS software to investigate the melting behavior of WC-reinforced H13 steel composite powder. Convection and radiation on the external skin while laser irradiation was incorporated in the model, and the thermal model was used to move Gaussian heat flow. The analytical modeling revealed that the relative proportions of WC and H13 steel powder substantially impacted the molten pool shape. The dispersion, packing efficiency, and absorption coefficient are the key point-of-process factors determining molten pool shape. Cardon, et al. [245] has studied experimental and simulated analyses of Ti-6Al-4 V materials using the SLM process. The numerical tool was developed to anticipate how heat treatment parameters (such as holding time and temperature) affect the residual stress field and distortions in SLM-produced components. The results indicated that the numerical and experimental distortions were evaluated for both sections, and the experimental and numerical data agreed correctly. Wu, et al. [246] studied the computational and experimental study of residual stress growth in AlSi10Mg materials fabricated in the

SLM technique. They used ABAQUS AM software to conduct the numerical analysis and developed a thermomechanical simulation to study the SLM processes temperature distribution and residual stress evolution. The results reveal that when the laser exposure period increases, residual stress within alloy portions increases. The discrepancy in residual stress between numerical simulation and experiment is less than 10%, of their stress linearity is highly similar, and the numerical technique used in this investigation was adequate. The working flowchart of the software is demonstrated in Fig. 26.

#### 7.5. Autodesk netfabb

Autodesk Netfabb is a server and physics-based multi-scale design software that predicts the thermomechanical behavior of printed parts and identifies deformations in a virtual environment [237]. Netfabb does not require a calibration process [235], and it is suitable for manipulating each AM machine parameter. Instead of the calibration process, this method requires creating a parameter file to define machine settings, scan pattern, and material characteristics (PRM file). Yilmaz and Kayacan [234] studied the effects of single and multiple part fabrication using a selective laser melting process. The sample's residual stress and displacement (distortions) were investigated by Autodesk Netfabb software, and the result showed that the maximum temperature values found from the experimental and FEA studies were well-matched. A piece of general information regarding Netfabb software is shown in Fig. 27.

#### 7.6. Additive Works Amphyon

Amphyon is user-friendly software with five modules in L-PBF chains from the CAD model through the build process, including stress-relieving and geometric distortion adjustment. [247]. The software also comprised various stages of the additive manufacturing process, like removing the build plate and secondary heat treatment, which can be possible [237]. Amphyon recommends that calibration is mandatory to get an accurate simulation of the process and a reliable prediction of stresses and distortion. The general information regarding the Amphyon software is depicted in Fig. 27 [235]. (Figs. 2, 7, 9, 13 and 28).

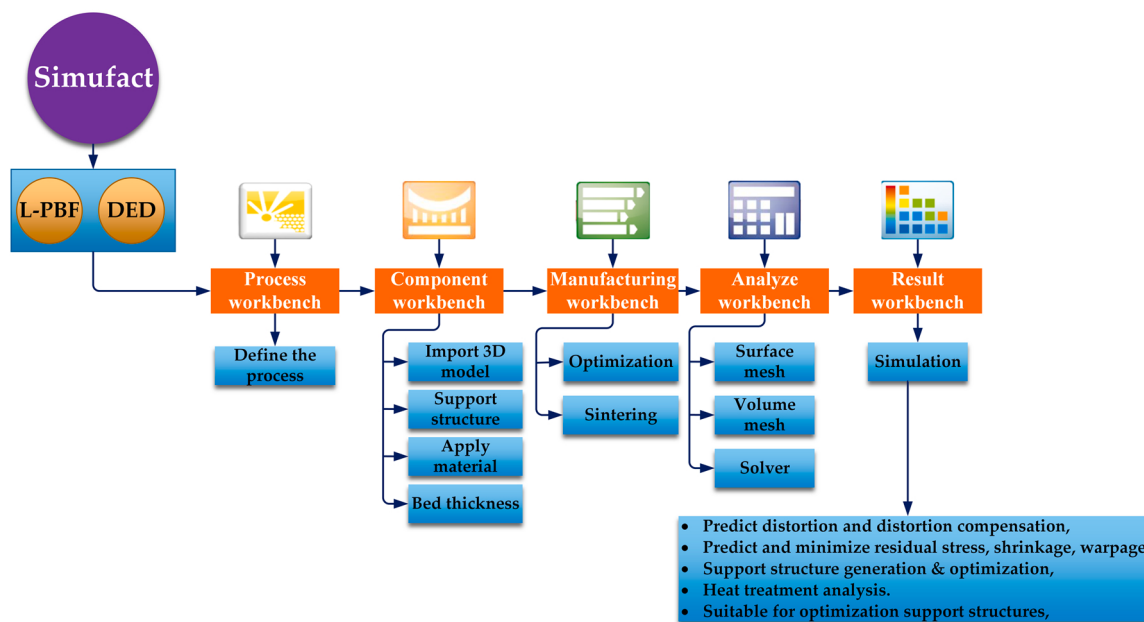


**Fig. 25.** Workflow and application of Simufact additive software [232, 235, 237, 239–241].

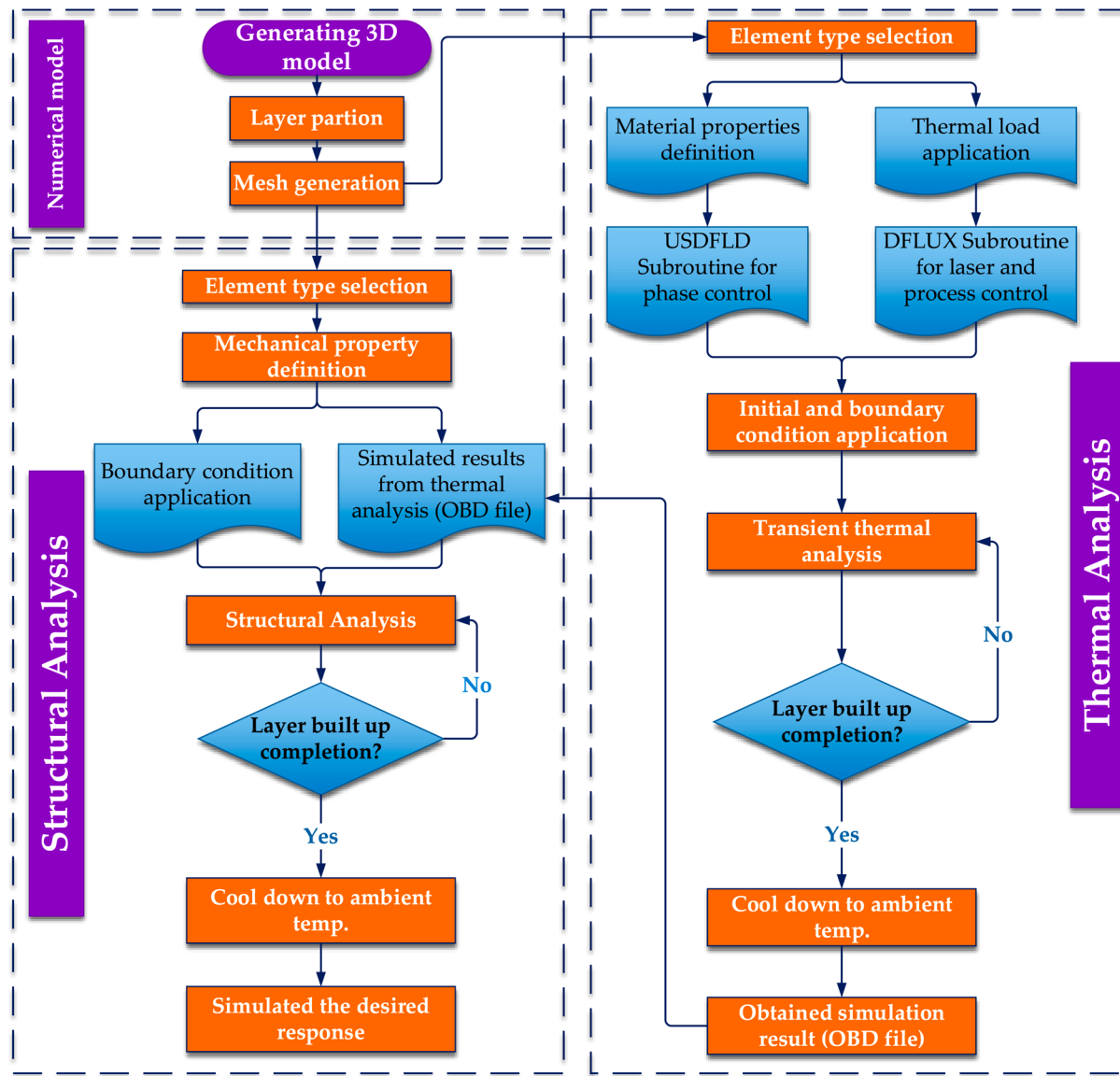
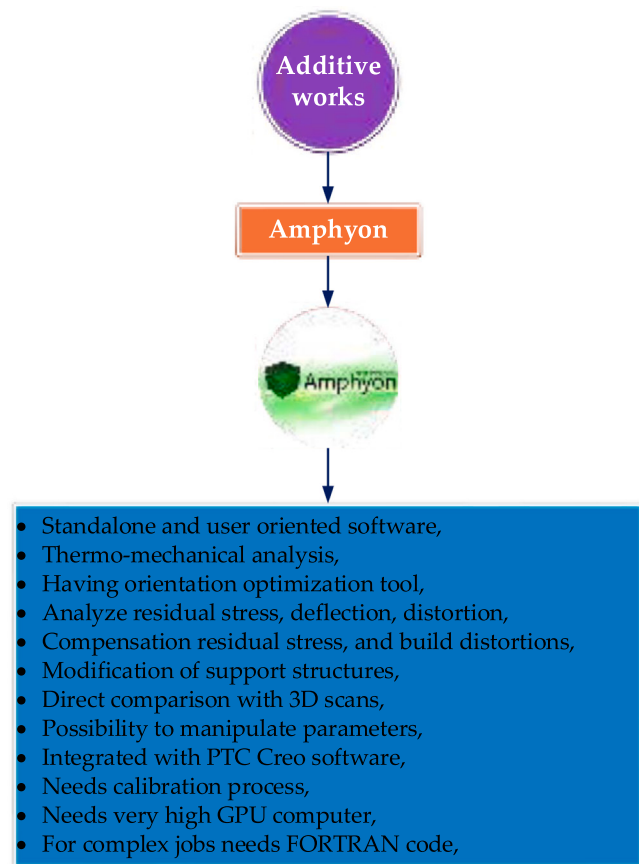
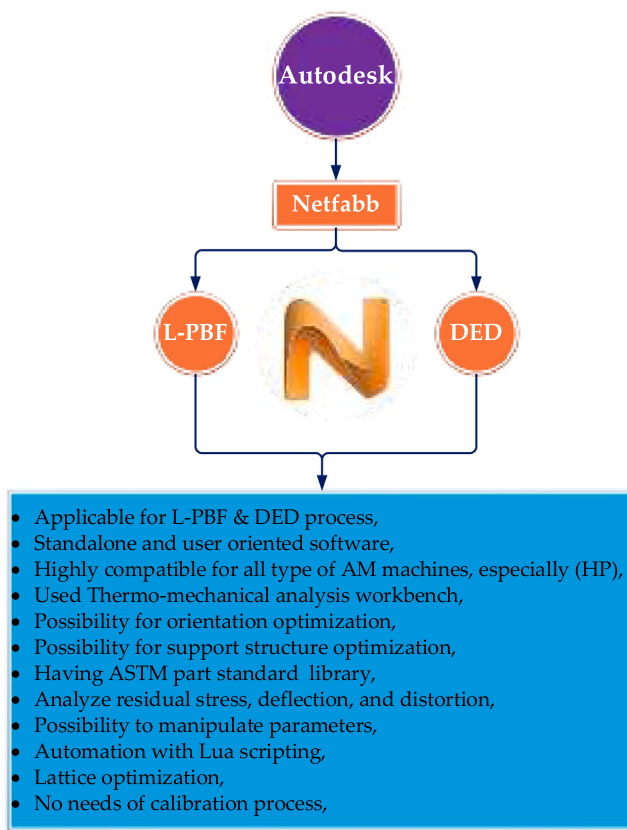


Fig. 26. ABAQUS AM flowchart [149].

### 7.7. Comsol multiphysics

Comsol is one of the multi-physics simulation tools from FE software. It can be demonstrated and used to analyze the SLM processes of laser absorption, conductive and convective heat transfer, and melting, solidification, evaporation, and condensation processes with the software. It is a parametric analysis tool and appropriate for optimizing the metal 3D printing process parameters, predicting the mechanical and microstructural properties of the printed part like final printed part, deformation, and stress analysis [237,248]. Afazov, et al. [249] utilized ABAQUS and COMSOL two FE software for investigated the distortion prediction and compensation of SS17-4 material using a selective laser melting process. They have developed two distortion compensation approaches and obtained good results compared to the experimental results. [250] has studied the process parameters, microstructure, and mechanical properties of SS316L and Al<sub>2</sub>O<sub>3</sub> materials using SLM processes. The powder has been agglomerated using a physical mixing in a roller mixer. They utilized Comsol multiphysics for modeling the part and assigned two powder materials in a single simulation. The simulation and experimentation findings indicated that a more significant laser energy input is required for optimal melting. Sharma and Kumar [251]

had investigated the thermal stress of Ti6Al4V material using SLM processes by developed a thermomechanical coupled model using Comsol software. The flowchart of the model has illustrated in Fig. 29. The thermo-mechanical simulation model bestowed a closed simulation result compared to the previous researcher's experimental results. Ye, et al. [252] a computational-based simulation was done using Comsol software to examine the joint effects of TiB<sub>2</sub> material on selective laser melting and chemical reactions in the Selective Laser Alloying (SLA) process. Their simulation used a low laser power of 35 W and a moderate scanning speed of 800 mm/sec. The simulation results indicate that the melting front of the free surface has a significantly higher velocity; the first speed jump occurs when the powder particles melt, and the second speed jump occurs whenever the reaction is triggered. The heat generated from the exothermic reaction among Titanium and Boron is a significant energy source that can reduce the energy input and help if the reaction is triggered. The heat released from the exothermic reaction among both Titanium and Boron is a significant energy source that can reduce the energy input and help enhance the SLA method's production efficiency. The temperature field in the computational domain is also influenced by latent evaporation heat. The concentration distribution of TiB<sub>2</sub> is highly influenced by the chemical reaction rate and the diffusion



coefficient.

## 8. Conclusions, limitations, and research outlook

Recent developments in the metal additive manufacturing process are becoming increasingly widespread in manufacturing industries and educational institutions. The focus of this review paper was on recent advances in the literature of a comprehensive analysis of the selective laser melting process. Because the process have a great demand in various industries and getting much attention, recent articles have been extensively reviewed to enhance the mechanical and metallurgical properties of the component that can be printed using the SLM method, and some of the key findings are included below:

- Understanding material property and process parameters are critically essential to print smart materials using the SLM process. Most smart materials are melted or fused within a small amount of laser power. So, low laser power, moderate scanning speed, and scanning strategies are crucial parameters for printing smart materials.
- It is challenging to print precious or reflective materials with ordinary SLM machines; it needs a moderate or customized SLM machine, components that resist the back reflective laser power. Printing the precious materials successfully, especially copper material, using high laser power, green laser type, and coating the printed materials with high laser absorbent characteristics materials, are the best alternative techniques.
- In the SLM process, multi-materials could modify mechanical, physical, and chemical characteristics, including hardness, electrical conductivity, magnetic permeability, corrosion resistance, and thermal conductivity. Bimetallic structures, as opposed to single-material structures, can provide unique engineering solutions. The selected material thermal properties, such as melting points, must be

close to each other unless the possibility of porosity occurrence among the interfacial line of the two materials is very high.

- Parameter optimization enhances the printed part quality; however, understanding each process parameter imparts a good quality product. All the process parameters are significant based on the study response; therefore, increasing or decreasing the magnitude of parameter levels must depend on the material properties and the required response study.
- Energy density is a critical factor that directly impacts the porosities and microstructures of as-built parts in the selective laser melting process. The characteristics of molten powder materials are determined by also the energy density process parameters. The power of energy density differs from material to material. Besides the energy density parameters, a combination of an ideal scanning strategy can significantly enhance the mechanical properties of the printed part.
- Build orientation is a crucial problem in the metal Am process because it is correlated to part accuracy, the amount of support required, and the processing time to fabricate the part. Selecting the optimal build orientation in the AM process will save fabrication expenses and increase part accuracy substantially. Netfabb, Netfabb, and Simufact additive having orientation optimization tool.
- To reduce printing costs and experimental tries with lattice structures, choose appropriate unit cell structures, materials, and process parameters that significantly influence the mechanical and microstructural lattice structures printed by the SLM technique.
- Post-processing is required after metal additive manufacturing processes to achieve the desired surface quality. Moreover, the selection of the post-processing process depends on the type of materials, geometry, and types of required surface quality.
- Support structures for overhanging components are necessary for SLM. These support structures serve as anchors and heat sinks,

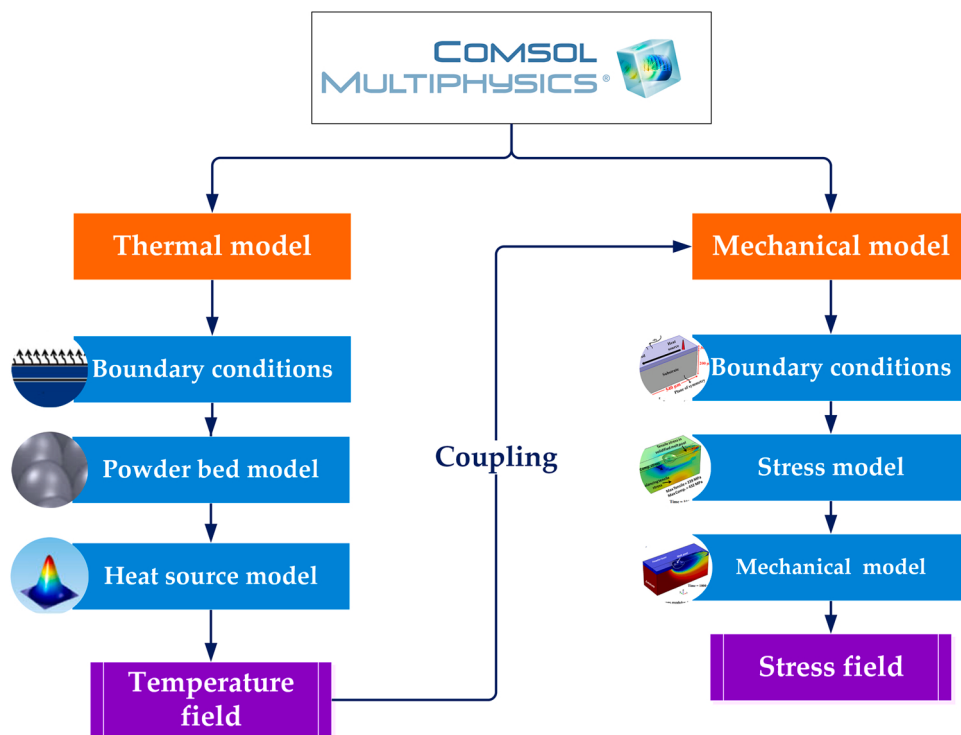


**Fig. 29.** Thermomechanical couplings of Comsol flowchart [251].

allowing excess heat to be dissipated. However, from an economic aspect, the use of a support structure is not recommended by the Design for Additive Manufacturing (DfAM). Currently, free contact support structures are utilized, and those are dual advantages on the mechanical property (reduction of distortions) and economic aspects; it employs fewer materials than a complete support structure. So, the utilization of support-free designs can minimize the consumption of materials and manufacturing time.

- Before going to AM machine, predicting the effects of selected process parameters on the response study of residual stress, deformation, and melt pool characteristics using FE software is crucial. Using Ansys Additive Print, Additive works Amphyon software, the company recommended a calibration process to obtain closer results to the experimental study. Besides, some packages require script coding to address the necessary parameters not mentioned in the software and complex works.

The fundamental drawback of this study is that it was primarily written based on the literature that is highly focused on the SLM process and metal materials and is not considered other AM processes and polymer materials. Various software is available in the SLM process; however, this study focused on the most reputable and extensively used by previous scholars.

The authors would like to recommend the following research areas to future scholars based on our state-of-the-art appraisal.

- **Printing of reflective materials:** Printing precious or reflective materials using the SLM process is complex due to the material absorbance of laser characteristics. So, research in this area is still restricted and requires sustainable printing solutions.
- **SLM Build speed:** SLM is one of the most promising AM processes for achieving the safest and more cost-effective manufacturing process. However, compared to other AM processes, the build speed of SLM is too slow. Nowadays, AM comes up with product development in so many application areas. Consequently, the process requires some

improvement in the build rate to improve the capability of mass production.

- **Composite materials:** Materials development for AM applications has advanced dramatically. The employment of composites or nanocomposite materials for performance improvement and flexibility is still restricted.
- **Multi-material:** The use of multi-materials in the SLM process is an infant. It needs further investigation in some specific points, like developing or customizing the current SLM machine physical feature and software upgrading and being commercialized. In addition, the process requires optimized process parameters for the combination materials.
- **Shrinkage mitigation:** SLM process imparts a near-net-shape product with a good surface finish. However, there is a slight difference between the printed part and the 3D CAD model known as metal shrinkage. So, the author would like to recommend utilizing AM software and support structures to mitigate shrinkages on the SLM printed part.
- **SLM process parameter and Defect correlations:** Past researchers studied SLM process parameter optimization and SLM defects very well. However, there is no research study on the SLM process parameters and their defect correlations.
- **Scanning strategy and energy density:** The effect of a scanning strategy including a combination of energy density on the morphological and mechanical properties has not been thoroughly investigated. Both parameters impact the response study; nevertheless, a combination of both parameters requires more research.

#### CRediT authorship contribution statement

**E.M.S.:** Conceptualization, Structure of the overall framework of the paper, Data curation, Methodology, Writing – original draft, Visualization, Review & editing the whole paper. The author has read and agreed to the published version of the manuscript.

## Declaration of Competing Interest

The author state that have no recognized competing financial interests or personal connections that might have influenced the research presented in this paper.

## References

- [1] Hernandez Korner ME, Lambán MP, Albajez JA, Santolaria J, Ng Corrales LDC, Royo J. Systematic literature review: integration of additive manufacturing and industry 4.0. Metals 2020;10(8):1061. <https://doi.org/10.3390/met10081061>.
- [2] Dilberoglu UM, Gharehpapagh B, Yaman U, Dolen M. The role of additive manufacturing in the era of industry 4.0. 2017/01/01/ Procedia Manuf 2017;11: 545–54. <https://doi.org/10.1016/j.promfg.2017.07.148>.
- [3] Alfaify A, Saleh M, Abdullah FM, Al-Ahmari AM. Design for additive manufacturing: a systematic review. Sustainability 2020;22. <https://doi.org/10.3390/su12197936>.
- [4] Santa-aho S, et al. Additive manufactured 316L stainless-steel samples: microstructure, residual stress and corrosion characteristics after post-processing. Metals 2021;11(2):15. <https://doi.org/10.3390/met11020182>.
- [5] Arbogast A, Roy S, Nyocz A, Noakes MW, Masuo C, Babu SS. Investigating the linear thermal expansion of additively manufactured multi-material joining between invar and steel. Materials 2020;13(24):5683. <https://doi.org/10.3390/ma13245683>.
- [6] V. Chaudhary, S.A. Mantri, R.V. Ramanujan, and R. Banerjee, "Additive manufacturing of magnetic materials," *Progress in Materials Science*, vol. 114, p. 100688, 2020/10/01/ 2020, doi: <https://doi.org/10.1016/j.pmatsci.2020.100688>.
- [7] S.A. M. Tofail, E.P. Koumoulos, A. Bandyopadhyay, S. Bose, L. O'Donoghue, and C. Charitidis, "Additive manufacturing: scientific and technological challenges, market uptake and opportunities," *Materials Today*, vol. 21, no. 1, pp. 22–37, 2018/01/01/ 2018, doi: <https://doi.org/10.1016/j.mattod.2017.07.001>.
- [8] Sefene EM, Hailu YM, Tsugaw AA. Metal hybrid additive manufacturing: state-of-the-art. 2022/01/31 Prog Addit Manuf 2022. <https://doi.org/10.1007/s40964-022-00262-1>.
- [9] A.K. Singla et al., "Selective laser melting of Ti6Al4V alloy: Process parameters, defects and post-treatments," *Journal of Manufacturing Processes*, vol. 64, pp. 161–187, 2021, doi: <https://doi.org/10.1016/j.jmapro.2021.01.009>.
- [10] Sturm LD, Williams CB, Camelio JA, White J, Parker R. "Cyber-physical vulnerabilities in additive manufacturing systems: a case study attack on the. STL file Hum Subj," *J Manuf Syst* 2017;44:154–64. <https://doi.org/10.1016/j.jmsy.2017.05.007>.
- [11] T.S. Leirmo and K. Martinsen, Evolutionary algorithms in additive manufacturing systems: Discussion of future prospects, *Procedia CIRP*, vol. 81, pp. 671–676, 2019, doi: <https://doi.org/10.1016/j.procir.2019.03.174>.
- [12] C. Gao, S. Wolff, and S. Wang, "Eco-friendly additive manufacturing of metals: Energy efficiency and life cycle analysis," *Journal of Manufacturing Systems*, vol. 60, pp. 459–472, 2021/07/01/ 2021, doi: <https://doi.org/10.1016/j.jmsy.2021.06.011>.
- [13] E. Atzeni and A. Salmi, Economics of additive manufacturing for end-useable metal parts, *The International Journal of Advanced Manufacturing Technology*, vol. 62, no. 9–12, pp. 1147–1155, 2012, doi: <http://doi.org/10.1007/s00170-011-3878-1>.
- [14] Fereiduni E, Ghasemi A, Elbestawi M. Selective laser melting of aluminum and titanium matrix composites: recent progress and potential applications in the aerospace industry. *Aerospace* 2020;7(6):77. <https://doi.org/10.3390/aerospace7060077>.
- [15] Zhang LC, Attar H. Selective laser melting of titanium alloys and titanium matrix composites for biomedical applications: a review. *Adv Eng Mater* 2016;18(4): 463–75. <https://doi.org/10.1002/adem.201500419>.
- [16] Song Y, Yan Y, Zhang R, Xu D, Wang F. Manufacture of the die of an automobile deck part based on rapid prototyping and rapid tooling technology. *J Mater Process Technol* 2002;120(1–3):237–42. [https://doi.org/10.1016/S0924-0136\(01\)01165-7](https://doi.org/10.1016/S0924-0136(01)01165-7).
- [17] Klocke F, et al. Turbomachinery component manufacture by application of electrochemical, electro-physical and photonic processes. 2014/01/01/ CIRP Ann 2014;63(2):703–26. <https://doi.org/10.1016/j.cirp.2014.05.004>.
- [18] A. Bandyopadhyay and B. Heer, "Additive manufacturing of multi-material structures," *Materials Science and Engineering: R: Reports*, vol. 129, pp. 1–16, 2018/07/01/ 2018, doi: <https://doi.org/10.1016/j.mser.2018.04.001>.
- [19] S. Mohd Yusuf, S. Cutler, and N. Gao, The impact of metal additive manufacturing on the aerospace industry, *Metals*, vol. 9, no. 12, p. 1286, 2019, doi: <https://doi.org/10.3390/met9121286>.
- [20] N. Nawafleh and E. Celik, Additive manufacturing of short fiber reinforced thermoset composites with unprecedented mechanical performance, *Additive Manufacturing*, vol. 33, p. 101109, 2020, doi: <https://doi.org/10.1016/j.addma.2020.101109>.
- [21] M. Attaran, The rise of 3-D printing: The advantages of additive manufacturing over traditional manufacturing, *Business Horizons*, vol. 60, no. 5, pp. 677–688, 2017, doi: <https://doi.org/10.1016/j.bushor.2017.05.011>.
- [22] S.D. Nath and S. Nilufar, "An Overview of Additive Manufacturing of Polymers and Associated Composites," *Polymers*, vol. 12, no. 11, p. 2719, 2020.
- [23] Y. Zhang et al., "Additive manufacturing of metallic materials: a review," *Journal of Materials Engineering Performance*, vol. 27, no. 1, pp. 1–13, 2018, doi: <https://doi.org/10.1007/s11665-017-2747-y>.
- [24] C. Liu, L. Le Roux, Z. Ji, P. Kerfriden, F. Lacan, and S. Bigot, Machine Learning-enabled feedback loops for metal powder bed fusion additive manufacturing, *Procedia Computer Science*, vol. 176, pp. 2586–2595, 2020, doi: <https://doi.org/10.1016/j.procs.2020.09.314>.
- [25] Kumar S. *Additive Manufacturing Processes*. Springer; 2020.
- [26] S. Hocine, H. Van Swygenhoven, and S. Van Petegem, "Verification of selective laser melting heat source models with operando X-ray diffraction data," *Additive Manufacturing*, vol. 37, p. 101747, 2021, doi: <https://doi.org/10.1016/j.addma.2020.101747>.
- [27] H. Neuberger et al., "Fabrication of HCPB breeding blanket components using the additive manufacturing processes of selective laser melting and cold spray," *Fusion Engineering and Design*, vol. 160, p. 112026, 2020, doi: <https://doi.org/10.1016/j.fusengdes.2020.112026>.
- [28] Zhou S, Su Y, Wang H, Enz J, Ebel T, Yan M. Selective laser melting additive manufacturing of 7xxx series Al-Zn-Mg-Cu alloy: cracking elimination by co-incorporation of Si and TiB2. *Addit Manuf* 2020;36:101458. <https://doi.org/10.1016/j.addma.2020.101458>.
- [29] Han Q, et al. Selective laser melting of Hastelloy X nanocomposite: effects of TiC reinforcement on crack elimination and strength improvement. 8442, 2020/12/01/ Compos Part B: Eng 2020;202:10. <https://doi.org/10.1016/j.compositesb.2020.108442>.
- [30] Biffi CA, Bassani P, Fiocchi J, Albu M, Tuissi A. Selective laser melting of AlCu-TiB2 alloy using pulsed wave laser emission mode: processability, microstructure and mechanical properties. *Mater Des* 2021;204:109628. <https://doi.org/10.1016/j.matedes.2021.109628>.
- [31] G.B. Bang et al., "Effect of process parameters for selective laser melting with SUS316L on mechanical and microstructural properties with variation in chemical composition," *Materials & Design*, vol. 197, p. 109221, 2021, doi: <https://doi.org/10.1016/j.matdes.2020.109221>.
- [32] S. Pauly et al., "Processing metallic glasses by selective laser melting," *Materials Today*, vol. 16, no. 1, pp. 37–41, 2013/01/01/ 2013, doi: <https://doi.org/10.1016/j.matto.2013.01.018>.
- [33] W. Zhai, Z. Zhu, W. Zhou, S.M. L. Nai, and J. Wei, "Selective laser melting of dispersed TiC particles strengthened 316L stainless steel," *Composites Part B: Engineering*, vol. 199, p. 108291, 2020/10/15/ 2020, doi: <https://doi.org/10.1016/j.compositesb.2020.108291>.
- [34] Yadroitsev I, Krakhmalev P, Yadroitsava I. Selective laser melting of Ti6Al4V alloy for biomedical applications: temperature monitoring and microstructural evolution. *J Alloy Compd* 2014;583:404–9. <https://doi.org/10.1016/j.jallcom.2013.08.183>.
- [35] Mertens R, Dadkhsh S, Van Humbeeck J, Kruth J-P. Application of base plate preheating during selective laser melting. *Procedia Cirp* 2018;74:5–11. <https://doi.org/10.1016/j.procir.2018.08.002>.
- [36] Chen W, Li Z. *Additive manufacturing of titanium aluminides (in). Additive Manufacturing for the Aerospace Industry*. Elsevier; 2019. p. 235–63 (in).
- [37] A. Gisario, M. Kazarian, F. Martina, and M. Mehrpouya, "Metal additive manufacturing in the commercial aviation industry: A review," *Journal of Manufacturing Systems*, vol. 53, pp. 124–149, 2019/10/01/ 2019, doi: <https://doi.org/10.1016/j.jmsy.2019.08.005>.
- [38] Sadali MF, Hassan MZ, Ahmad F, Yahaya H, Rasid ZA. Influence of selective laser melting scanning speed parameter on the surface morphology, surface roughness, and micropores for manufactured Ti6Al4V parts. *J Mater Res* 2020;35(15): 2025–35. <https://doi.org/10.1557/jmr.2020.84>.
- [39] Singh S, Ramakrishna S, Singh R. Material issues in additive manufacturing: a review. *J Manuf Process* 2017;25:185–200. <https://doi.org/10.1016/j.jmapro.2016.11.006>.
- [40] Zocca A, Colombo P, Gomes CM, Günster J. Additive manufacturing of ceramics: issues, potentialities, and opportunities. *J Am Ceram Soc* 2015;98(7):1983–2001. <https://doi.org/10.1111/jace.13700>.
- [41] Zhang B, Li Y, Bai Q. Defect formation mechanisms in selective laser melting: a review. *Chin J Mech Eng* 2017;30(3):515–27. <https://doi.org/10.1007/s10033-017-0121-5>.
- [42] S.M. Tawfik, M.N. Nasr, and H.A. El Gamal, "Finite element modelling for part distortion calculation in selective laser melting," *Alexandria Engineering Journal*, vol. 58, no. 1, pp. 67–74, 2019, doi: <https://doi.org/10.1016/j.aej.2018.12.010>.
- [43] Gheysen J, Marteleur M, van der Rest C, Simar A. Efficient optimization methodology for laser powder bed fusion parameters to manufacture dense and mechanically sound parts validated on AlSi12 alloy. *Mater Des* 2021;199:109433. <https://doi.org/10.1016/j.matedes.2020.109433>.
- [44] Wu Y, Sun K, Yu S, Zuo L. Modeling the selective laser melting-based additive manufacturing of thermoelectric powders. *Addit Manuf* 2021;37:101666. <https://doi.org/10.1016/j.addma.2020.101666>.
- [45] Patterson AE, Messimer SL, Farrington PA. Overhanging features and the SLM/DMLS residual stresses problem: review and future research need. *Technologies* 2017;vol. 5(2):15. <https://doi.org/10.3390/technologies5020015>.
- [46] Popov VV, et al. Powder bed fusion additive manufacturing using critical raw materials: a review. *Materials* 2021;14(4):909. <https://doi.org/10.3390/ma14040909>.
- [47] Balbaa M, Ghasemi A, Fereiduni E, Elbestawi M, Jadhav S, Kruth J-P. Role of powder particle size on laser powder bed fusion processability of AlSi10mg alloy. *Addit Manuf* 2021;37:101630. <https://doi.org/10.1016/j.addma.2020.101630>.
- [48] Haferkamp L, et al. The influence of particle shape, powder flowability, and powder layer density on part density in laser powder bed fusion. *Metals* 2021;vol. 11(3):418. <https://doi.org/10.3390/met11030418>.

- [49] Haferkamp L, Spierings A, Rusch M, Jermann D, Spurek MA, Wegener K. Effect of particle size of monomodal 316L powder on powder layer density in powder bed fusion. *Prog Addit Manuf* 2020;1:8. <https://doi.org/10.1007/s40964-020-00152-4>.
- [50] Baitimerov R, Lykov P, Zherebtsov D, Radionova L, Shultz A, Prashanth KG. Influence of powder characteristics on processability of AlSi12 alloy fabricated by selective laser melting. *Materials* 2018;11(5):742. <https://doi.org/10.3390/mal11050742>.
- [51] P.A. Kuznetsov, I.V. Shakirov, A.S. Zukov, V.V. Bobyr', and M.V. Staritsin, "Effect of particle size distribution on the structure and mechanical properties in the process of laser powder bed fusion," *Journal of Physics: Conference Series*, vol. 1758, p. 012021, 2021/01 2021, doi: <https://doi.org/10.1088/1742-6596/1758/1/012021>.
- [52] C. Pleass and S. Jothi, "Influence of powder characteristics and additive manufacturing process parameters on the microstructure and mechanical behaviour of Inconel 625 fabricated by Selective Laser Melting," *Additive Manufacturing*, vol. 24, pp. 419–431, 2018/12/01/ 2018, doi: <https://doi.org/10.1016/j.addma.2018.09.023>.
- [53] Spierings AB, Herres N, Levy G. Influence of the particle size distribution on surface quality and mechanical properties in AM steel parts (doi: <https://DOI.org/>) *Rapid Prototyp J* 2011. <https://doi.org/10.1108/13552541111124770>.
- [54] Zhang J, et al. Influence of particle size on laser absorption and scanning track formation mechanisms of pure tungsten powder during selective laser melting. 2019/08/01/ *Engineering* 2019;5(4):736–45. <https://doi.org/10.1016/j.eng.2019.07.003>.
- [55] Choi J-P, et al. Evaluation of powder layer density for the selective laser melting (SLM) process. *Mater Trans* 2017;58(2):294–7. <https://doi.org/10.2320/matertrans.M2016364>.
- [56] Riener K, et al. Influence of particle size distribution and morphology on the properties of the powder feedstock as well as of AlSi10Mg parts produced by laser powder bed fusion (LPBF). 2020/08/01/ *Addit Manuf* 2020;34:101286. <https://doi.org/10.1016/j.addma.2020.101286>.
- [57] Y. Sun, S. Gulizia, C. Oh, C. Doblin, Y.F. Yang, and M. Qian, Manipulation and characterization of a novel titanium powder precursor for additive manufacturing applications, *Jom*, vol. 67, no. 3, pp. 564–572, 2015, doi: <https://DOI.org/10.1007/s11837-015-1301-3>.
- [58] Muñiz-Lerma JA, Nommeots-Nomm A, Waters KE, Brochu M. A comprehensive approach to powder feedstock characterization for powder bed fusion additive manufacturing: a case study on AlSi7Mg. *Materials* 2018;vol. 11(12):2386. <https://doi.org/10.3390/ma11122386>.
- [59] H.G. Coe and S. Pasebani, Use of bimodal particle size distribution in selective laser melting of 316L stainless steel, *Journal of Manufacturing and Materials Processing*, vol. 4, no. 1, p. 8, 2020, doi: <https://doi.org/10.3390/jmmp4010008>.
- [60] Popozov I, Popovich A. Microstructure and mechanical properties of niti-based eutectic shape memory alloy produced via selective laser melting in-situ alloying by Nb. *Materials* 2021;14(10):2696. <https://doi.org/10.3390/ma14102696>.
- [61] K.G. Prashanth, S. Scudino, and J. Eckert, "Defining the tensile properties of Al-12Si parts produced by selective laser melting," *Acta Materialia*, vol. 126, pp. 25–35, 2017/03/01/ 2017, doi: <https://doi.org/10.1016/j.actamat.2016.12.044>.
- [62] L.C. Ardila et al., "Effect of IN718 Recycled Powder Reuse on Properties of Parts Manufactured by Means of Selective Laser Melting," *Physics Procedia*, vol. 56, pp. 99–107, 2014/01/01/ 2014, doi: <https://doi.org/10.1016/j.phpro.2014.08.152>.
- [63] Y. Li, K. Zhou, S.B. Tor, C.K. Chua, and K.F. Leong, "Heat transfer and phase transition in the selective laser melting process," *International Journal of Heat and Mass Transfer*, vol. 108, pp. 2408–2416, 2017/05/01/ 2017, doi: <https://doi.org/10.1016/j.ijheatmasstransfer.2017.01.093>.
- [64] Mazur M, Benoit M, Easton M, Brandt M. Selective laser melting of Inconel 625 alloy with reduced defect formation. *J Laser Appl* 2020;32(2):022058. <https://doi.org/10.2351/7.000093>.
- [65] C. Fleißner-Rieger et al., Selective Laser Melting of a Near- $\alpha$  Ti6242S Alloy for High Performance Automotive Parts, *Advanced Engineering Materials*, doi: <https://doi.org/10.1002/adem.202001194>.
- [66] Martin JH, Yahata BD, Hundley JM, Mayer JA, Schaebler TA, Pollock TM. 3D printing of high-strength aluminium alloys. *Nature* 2017;549(7672):365–9. <https://doi.org/10.1038/nature23894>.
- [67] Chekotu JC, Groarke R, O'Toole K, Brabazon D. Advances in selective laser melting of nitinol shape memory alloy part production. *Materials* 2019;12(5):809. <https://doi.org/10.3390/ma12050809>.
- [68] M. Taheri Andani et al., "Mechanical and shape memory properties of porous Ni50.1Ti49.9 alloys manufactured by selective laser melting," *Journal of the Mechanical Behavior of Biomedical Materials*, vol. 68, pp. 224–231, 2017/04/01/ 2017, doi: <https://doi.org/10.1016/j.jmbbm.2017.01.047>.
- [69] M. Mehroouya, A. Gisario, M. Nematollahi, A. Rahimzadeh, K.S. Baghbaderani, and M. Elahinia, "The prediction model for additively manufacturing of NiTiHf high-temperature shape memory alloy," *Materials Today Communications*, vol. 26, p. 102022, 2021/03/01/ 2021, doi: <https://doi.org/10.1016/j.mtcomm.2021.102022>.
- [70] Liu G, et al. Additive manufacturing of structural materials. 2021/07/01/ *Mater Sci Eng: R: Rep* 2021;145:100596. <https://doi.org/10.1016/j.mser.2020.100596>.
- [71] Khoob ZX, Liu Y, Low ZH, An J, Chua CK, Leong KF. Fabrication of SLM NiTi shape memory alloy via repetitive laser scanning. *Shape Mem Superelasticity* 2018;4(1):112–20. <https://doi.org/10.1007/s40830-017-0139-7>.
- [72] Wang X, et al. Effect of process parameters on the phase transformation behavior and tensile properties of NiTi shape memory alloys fabricated by selective laser melting. 2020/12/01/ *Addit Manuf* 2020;36:101545. <https://doi.org/10.1016/j.addma.2020.101545>.
- [73] Xiong Z, et al. Selective laser melting of NiTi alloy with superior tensile property and shape memory effect. 2019/10/01/ *J Mater Sci Technol* 2019;35(10):2238–42. <https://doi.org/10.1016/j.jmst.2019.05.015>.
- [74] J. Chen, Y. Yang, C. Song, D. Wang, S. Wu, and M. Zhang, "Influence mechanism of process parameters on the interfacial characterization of selective laser melting 316L/CuSn10," *Materials Science and Engineering: A*, vol. 792, p. 139316, 2020/08/05/ 2020, doi: <https://doi.org/10.1016/j.msea.2020.139316>.
- [75] A.G. Demir and B. Previtali, "Multi-material selective laser melting of Fe/Al-12Si components," *Manufacturing Letters*, vol. 11, pp. 8–11, 2017/01/01/ 2017, doi: <https://doi.org/10.1016/j.mfglet.2017.01.002>.
- [76] C. Wei, L. Li, X. Zhang, and Y.-H. Chueh, "3D printing of multiple metallic materials via modified selective laser melting," *CIRP Annals*, vol. 67, no. 1, pp. 245–248, 2018/01/01/ 2018, doi: <https://doi.org/10.1016/j.cirp.2018.04.096>.
- [77] Wei C, Sun Z, Chen Q, Liu Z, Li L. Additive manufacturing of horizontal and 3D functionally graded 316L/Cu10Sn components via multiple material selective laser melting (<https://DOI.org/>) *J Manuf Sci Eng* 2019;141(8). <https://doi.org/10.1115/1.4043983>.
- [78] S.L. Sing, L.P. Lam, D.Q. Zhang, Z.H. Liu, and C.K. Chua, "Interfacial characterization of SLM parts in multi-material processing: Intermetallic phase formation between AlSi10Mg and C18400 copper alloy," *Materials Characterization*, vol. 107, pp. 220–227, 2015/09/01/ 2015, doi: <https://doi.org/10.1016/j.matchar.2015.07.007>.
- [79] Costa MM, et al. Multi-material NiTi-PEEK hybrid cellular structures by selective laser melting and hot pressing: tribological characterization. 2021/04/01/ *Tribology Int* 2021;156:106830. <https://doi.org/10.1016/j.triboint.2020.106830>.
- [80] I. Miyamoto and G.A. Knorovsky, "14 - Laser microwelding," in *Microjoining and Nanojoining*, Y. Zhou Ed.: Woodhead Publishing, 2008, pp. 345–417.
- [81] Jadhav SD, et al. Laser powder bed fusion additive manufacturing of highly conductive parts made of optically absorptive carburized CuCr1 powder. 2021/01/15/ *Mater Des* 2021;vol. 198:109369. <https://doi.org/10.1016/j.matedes.2020.109369>.
- [82] Naeem M. Laser processing of reflective materials: a new technology managing reflection effects. *Laser Tech J* 2013;10(1):18–20. <https://doi.org/10.1002/latj.20139001>.
- [83] P. Lassègue et al., Laser powder bed fusion (L-PBF) of Cu and CuCrZr parts: Influence of an absorptive physical vapor deposition (PVD) coating on the printing process, *Additive Manufacturing*, vol. 39, p. 101888, 2021, doi: <https://doi.org/10.1016/j.addma.2021.101888>.
- [84] V. Lindström et al., "Laser Powder Bed Fusion of Metal Coated Copper Powders," *Materials*, vol. 13, no. 16, p. 3493, 2020, doi: <https://doi.org/10.3390/ma13163493>.
- [85] A. Hess, R. Schuster, A. Heider, R. Weber, and T. Graf, "Continuous Wave Laser Welding of Copper with Combined Beams at Wavelengths of 1030nm and of 515nm," *Physics Procedia*, vol. 12, pp. 88–94, 2011/01/01/ 2011, doi: <https://doi.org/10.1016/j.phpro.2011.03.012>.
- [86] Prasad HS, Brueckner F, Volpp J, Kaplan AF. Laser metal deposition of copper on diverse metals using green laser sources. *Int J Adv Manuf Technol* 2020;107(3):1559–68. <https://doi.org/10.1007/s00170-020-05117-z>.
- [87] Jadhav SD, et al. Highly conductive and strong CuSn0.3 alloy processed via laser powder bed fusion starting from a tin-coated copper powder. 2020/12/01/ *Addit Manuf* 2020;36:101607. <https://doi.org/10.1016/j.addma.2020.101607>.
- [88] Sames WJ, List F, Pannala S, Dehoff RR, Babu SS. The metallurgy and processing science of metal additive manufacturing. *Int Mater Rev* 2016;61(5):315–60. <https://doi.org/10.1080/09506608.2015.1116649>.
- [89] Sing SL, et al. Emerging metallic systems for additive manufacturing: in-situ alloying and multi-metal processing in laser powder bed fusion. 2021/06/01/ *Prog Mater Sci* 2021;119:100795. <https://doi.org/10.1016/j.pmatsci.2021.100795>.
- [90] S.K. Everton, M. Hirsch, P. Stravroulakis, R.K. Leach, and A.T. Clare, "Review of in-situ process monitoring and in-situ metrology for metal additive manufacturing," *Materials & Design*, vol. 95, pp. 431–445, 2016/04/05/ 2016, doi: <https://doi.org/10.1016/j.matdes.2016.01.099>.
- [91] Prashanth KG, Scudino S, Maity T, Das J, Eckert J. Is the energy density a reliable parameter for materials synthesis by selective laser melting? *Mater Res Lett* 2017;5(6):386–90. doi: <https://doi.org/10.1080/21663831.2017.1299808>.
- [92] Levkulich N, Semiatin S, Gockel J, Middendorf J, DeWald A, Klingbeil N. The effect of process parameters on residual stress evolution and distortion in the laser powder bed fusion of Ti-6Al-4V. *Addit Manuf* 2019;28:475–84. <https://doi.org/10.1016/j.addma.2019.05.015>.
- [93] D. Grossin et al., "A review of additive manufacturing of ceramics by powder bed selective laser processing (sintering/melting): Calcium phosphate, silicon carbide, zirconia, alumina, and their composites," *Open Ceramics*, p. 100073, 2021, doi: <https://doi.org/10.1016/j.oceram.2021.100073>.
- [94] Wang H, Wang L, Cui R, Wang B, Luo L, Su Y. Differences in microstructure and nano-hardness of selective laser melted Inconel 718 single tracks under various melting modes of molten pool. *J Mater Res Technol* 2020;9(5):10401–10. <https://doi.org/10.1016/j.jmrt.2020.07.029>.
- [95] Di W, Yongqiang Y, Xubin S, Yonghua C. Study on energy input and its influences on single-track, multi-track, and multi-layer in SLM (<https://DOI.org/>) *Int J Adv Manuf Technol* 2022;58(9):1189–99. <https://doi.org/10.1007/s00170-011-3443-y>.

- [96] P. Huo, Z. Zhao, W. Du, Z. Zhang, P. Bai, and D. Tie, "Deformation strengthening mechanism of in situ TiC/TC4 alloy nanocomposites produced by selective laser melting," *Composites Part B: Engineering*, vol. 225, p. 109305, 2021/11/15/ 2021, doi: (<https://doi.org/10.1016/j.compositesb.2021.109305>).
- [97] Averyanova M, Bertrand P, Verquin B. Studying the influence of initial powder characteristics on the properties of final parts manufactured by the selective laser melting technology: a detailed study on the influence of the initial properties of various martensitic stainless steel powders on the final microstructures and mechanical properties of parts manufactured using an optimized SLM process is reported in this paper. *Virtual Phys Prototyp* 2011;6(4):215–23. <https://doi.org/10.1080/17452759.2011.594645>.
- [98] N.T. Aboulkhair, M. Simonelli, L. Parry, I. Ashcroft, C. Tuck, and R. Hague, "3D printing of Aluminium alloys: Additive Manufacturing of Aluminium alloys using selective laser melting," *Progress in Materials Science*, vol. 106, p. 100578, 2019/12/01/ 2019, doi: (<https://doi.org/10.1016/j.pmatsci.2019.100578>).
- [99] Kumar LJ, Pandey PM, Wimpenny DI. *3D printing and additive manufacturing technologies*. Springer; 2018.
- [100] Peng T, Chen C. Influence of energy density on energy demand and porosity of 316L stainless steel fabricated by selective laser melting (<https://DOI.org/>) *Int J Precis Eng Manuf-Green Technol* 2018;5(1):55–62. <https://doi.org/10.1007/s40684-018-0006-9>.
- [101] Donik J, Kranner I, Paulin, Godec M. Influence of the energy density for selective laser melting on the microstructure and mechanical properties of stainless steel. *Metals* 2020;10(7):919. <https://doi.org/10.3390/met10070919> (C).
- [102] Bertoli US, Wolfer AJ, Matthews MJ, Delplanque J-PR, Schoenung JM. On the limitations of volumetric energy density as a design parameter for selective laser melting. *Mater Des* 2017;113:331–40. <https://doi.org/10.1016/j.matdes.2016.10.037>.
- [103] Wu H, et al. Effect of melting modes on microstructure and tribological properties of selective laser melted AlSi10Mg alloy. *Virtual Phys Prototyp* 2020;15(sup1): 570–82. <https://doi.org/10.1080/17452759.2020.1811932>.
- [104] Ren Y, et al. Effect of volumetric energy density on microstructure and tribological properties of FeCoNiCuAl high-entropy alloy produced by laser powder bed fusion. *Virtual Phys Prototyp* 2020;15(sup1):543–54. <https://doi.org/10.1080/17452759.2020.1848284>.
- [105] Wang J, Liu S, Fang Y, He Z. A short review on selective laser melting of H13 steel. *Int J Adv Manuf Technol* 2020;108:2453–66. <https://doi.org/10.1007/s00170-020-05584-4>.
- [106] Liu J, et al. Effect of scanning speed on the microstructure and mechanical behavior of 316L stainless steel fabricated by selective laser melting. *Mater Des* 2020;vol. 186:108355. <https://doi.org/10.1016/j.matdes.2019.108355>.
- [107] Xiong W, et al. Effect of selective laser melting parameters on morphology, microstructure, densification and mechanical properties of supersaturated silver alloy. *Mater Des* 2019;170:107697. <https://doi.org/10.1016/j.matdes.2019.107697>.
- [108] Kang J, Yi J, Wang T. Effect of laser power and scanning speed on the microstructure and mechanical properties of SLM fabricated Inconel 718 specimens. *Mater Sci Eng* 2019;3:72–6. <https://doi.org/10.15406/msej.2019.03.00094>.
- [109] Miao X, Liu X, Lu P, Han J, Duan W, Wu M. Influence of scanning strategy on the performances of GO-reinforced Ti6Al4V nanocomposites manufactured by SLM. *Metals* 2020;10(10):1379. <https://doi.org/10.3390/met10101379>.
- [110] Yuan W, Chen H, Cheng T, Wei Q. Effects of laser scanning speeds on different states of the molten pool during selective laser melting: simulation and experiment. *Mater Des* 2020;189:108542. <https://doi.org/10.1016/j.matdes.2020.108542>.
- [111] Enneti RK, Morgan R, Atre SV. Effect of process parameters on the selective laser melting (SLM) of tungsten. *Int J Refract Met Hard Mater* 2018;71:315–9. <https://doi.org/10.1016/j.ijrmhm.2017.11.035>.
- [112] Maamoun AH, Xue YF, Elbestawi MA, Veldhuis SC. Effect of selective laser melting process parameters on the quality of al alloy parts: powder characterization, density, surface roughness, and dimensional accuracy. *Materials* 2018;11(12):2343. <https://doi.org/10.3390/ma11122343>.
- [113] Bremen S, Meiners W, Diatlov A. Selective laser melting: a manufacturing technology for the future? *Laser Tech J* 2012;9(2):33–8. <https://doi.org/10.1002/latj.201290018>.
- [114] Amirjan M, Sakiani H. Effect of scanning strategy and speed on the microstructure and mechanical properties of selective laser melted IN718 nickel-based superalloy. *Int J Adv Manuf Technol* 2019;103(5):1769–80. <https://doi.org/10.1007/s00170-019-03545-0>.
- [115] Eliasus A, Czekanski A, Boakye-Yiadom S. Effect of laser powder bed fusion parameters on the microstructural evolution and hardness of 316L stainless steel. *Int J Adv Manuf Technol* 2021;113(9):2651–69. <https://doi.org/10.1007/s00170-021-06818-9>.
- [116] Oyesola M, Mpofu K, Mathe N, Fatoba S, Hoosain S, Daniyan I. Optimization of selective laser melting process parameters for surface quality performance of the fabricated Ti6Al4V. *Int J Adv Manuf Technol* 2021;114(5):1585–99. <https://doi.org/10.1007/s00170-021-06953-3>.
- [117] Greco S, Gutzeit K, Hotz H, Kirsch B, Aurich JC. Selective laser melting (SLM) of AISI 316L—impact of laser power, layer thickness, and hatch spacing on roughness, density, and microhardness at constant input energy density. *Int J Adv Manuf Technol* 2020;108:1551–62. <https://doi.org/10.1007/s00170-020-05510-8>.
- [118] Dong Z, Liu Y, Wen W, Ge J, Liang J. Effect of hatch spacing on melt pool and as-built quality during selective laser melting of stainless steel: Modeling and experimental approaches. *Materials* 2019;12(1):50. <https://doi.org/10.3390/ma2010050>.
- [119] J. Huang, M. Li, J. Wang, Z. Pei, P. McIntyre, and C. Ma, "Selective laser melting of tungsten: Effects of hatch distance and point distance on pore formation," *Journal of Manufacturing Processes*, vol. 61, pp. 296–302, 2021/01/01/ 2021, doi: <https://doi.org/10.1016/j.jmapro.2020.11.034>.
- [120] S. Wang et al., "Research on high layer thickness fabricated of 316L by selective laser melting," *Materials*, vol. 10, no. 9, p. 1055, 2017, doi: (<https://doi.org/10.3390/ma10091055>).
- [121] E.O. Olakanmi, R.F. Cochrane, and K.W. Dalgarno, "A review on selective laser sintering/melting (SLS/SLM) of aluminium alloy powders: Processing, microstructure, and properties," *Progress in Materials Science*, vol. 74, pp. 401–477, 2015/10/01/ 2015, doi: (<https://doi.org/10.1016/j.pmatsci.2015.03.002>).
- [122] J. Robinson, I. Ashton, P. Fox, E. Jones, and C. Sutcliffe, "Determination of the effect of scan strategy on residual stress in laser powder bed fusion additive manufacturing," *Additive Manufacturing*, vol. 23, pp. 13–24, 2018/10/01/ 2018, doi: (<https://doi.org/10.1016/j.addma.2018.07.001>).
- [123] J. Jhabvala, E. Boillat, T. Antignac, and R. Glardon, On the effect of scanning strategies in the selective laser melting process, *Virtual and physical prototyping*, vol. 5, no. 2, pp. 99–109, 2010, doi: <https://DOI.org/10.1080/17452751003688368>.
- [124] N.T. Aboulkhair, N.M. Everitt, I. Ashcroft, and C. Tuck, "Reducing porosity in AlSi10Mg parts processed by selective laser melting," *Additive Manufacturing*, vol. 1–4, pp. 77–86, 2014/10/01/ 2014, doi: (<https://doi.org/10.1016/j.addma.2014.08.001>).
- [125] Jia H, Sun H, Wang H, Wu Y, Wang H. Scanning strategy in selective laser melting (SLM): a review. *Int J Adv Manuf Technol* 2021;1–23. <https://doi.org/10.1007/s00170-021-06810-3>.
- [126] P. Nandwana and Y. Lee, "Influence of scan strategy on porosity and microstructure of Ti-6Al-4V fabricated by electron beam powder bed fusion," *Materials Today Communications*, vol. 24, p. 100962, 2020/09/01/ 2020, doi: (<https://doi.org/10.1016/j.mtcomm.2020.100962>).
- [127] B. AlMangour, D. Grzesiak, and J.-M. Yang, "Scanning strategies for texture and anisotropy tailoring during selective laser melting of TiC/316L stainless steel nanocomposites," *Journal of Alloys and Compounds*, vol. 728, pp. 424–435, 2017/12/25/ 2017, doi: <https://doi.org/10.1016/j.jallcom.2017.08.022>.
- [128] Mercelis P, Kruth JP. Residual stresses in selective laser sintering and selective laser melting. *Rapid Prototyp J* 2006. <https://doi.org/10.1108/13552540610707013>.
- [129] Zaeih MF, Branner G. Investigations on residual stresses and deformations in selective laser melting. *Prod Eng* 2010;14(1):35–45. <https://doi.org/10.1007/s11740-009-0192-y>.
- [130] Kruth JP, Deckers J, Yasa E, Wauthlé R. Assessing and comparing influencing factors of residual stresses in selective laser melting using a novel analysis method (doi: <https://DOI.org/>) *Proc Inst Mech Eng, Part B: J Eng Manuf* 2012;226(6): 980–91. <https://doi.org/10.1177/0954405412437085>.
- [131] H.Y. Wan, Z.J. Zhou, C.P. Li, G.F. Chen, and G.P. Zhang, "Effect of scanning strategy on mechanical properties of selective laser melted Inconel 718," *Materials Science and Engineering: A*, vol. 753, pp. 42–48, 2019/04/10/ 2019, doi: (<https://doi.org/10.1016/j.msea.2019.03.007>).
- [132] J. Karimi, C. Suryanarayana, I. Okulov, and K.G. Prashanth, "Selective laser melting of Ti6Al4V: Effect of laser re-melting," *Materials Science and Engineering: A*, vol. 805, p. 140558, 2021/02/23/ 2021, doi: (<https://doi.org/10.1016/j.msea.2020.140558>).
- [133] Q. He, H. Xia, J. Liu, X. Ao, and S. Lin, "Modeling and numerical studies of selective laser melting: Multiphase flow, solidification and heat transfer," *Materials & Design*, vol. 196, p. 109115, 2020/11/01/ 2020, doi: (<https://doi.org/10.1016/j.mtades.2020.109115>).
- [134] R. Rashid et al., "Effect of energy per layer on the anisotropy of selective laser melted AlSi12 aluminium alloy," *Additive Manufacturing*, vol. 22, pp. 426–439, 2018/08/01/ 2018, doi: (<https://doi.org/10.1016/j.addma.2018.05.040>).
- [135] Mfusi B, Tshabalala LC, Popoola A, Mathe NR. The effect of selective laser melting build orientation on the mechanical properties of AlSi10Mg parts," in: *IOP Conference Series: Materials Science and Engineering*, 430, IOP Publishing; 2018.
- [136] M. Simonelli, Y.Y. Tse, and C. Tuck, "Effect of the build orientation on the mechanical properties and fracture modes of SLM Ti-6Al-4V," *Materials Science and Engineering: A*, vol. 616, pp. 1–11, 2014/10/20/ 2014, doi: (<https://doi.org/10.1016/j.msea.2014.07.086>).
- [137] P. Hartunian and M. Eshraghi, Effect of build orientation on the microstructure and mechanical properties of selective laser-melted Ti-6Al-4V alloy, *Journal of Manufacturing and Materials Processing*, vol. 2, no. 4, p. 69, 2018, doi: (<https://doi.org/10.3390/jmmp2040069>).
- [138] Shumugavel M, Polishetty A, Goldberg M, Nomani J, Littlefair G. Influence of build orientation on machinability of selective laser melted titanium alloy-Ti-6Al-4V. *World Acad Sci, Eng Technol, Int J Chem, Mol, Nucl, Mater Metall Eng* 2017; 11:515–9.
- [139] D.S. Nguyen, H.S. Park, and C.M. Lee, Optimization of selective laser melting process parameters for Ti-6Al-4V alloy manufacturing using deep learning, *Journal of Manufacturing Processes*, vol. 55, pp. 230–235, 2020, doi: (<https://doi.org/10.1016/j.jmapro.2020.04.014>).
- [140] A. Fatemi, R. Molaei, S. Sharifimehr, N. Phan, and N. Shamsaei, "Multiaxial fatigue behavior of wrought and additive manufactured Ti-6Al-4V including surface finish effect," *International Journal of Fatigue*, vol. 100, pp. 347–366, 2017/07/01/ 2017, doi: (<https://doi.org/10.1016/j.ijfatigue.2017.03.044>).

- [141] L. Wan et al., "Parameter optimization of selective laser melting fabricated titanium alloy using skin-core and triple contour scanning strategy," *Journal of Laser Applications*, vol. 32, no. 4, p. 042001, 2020, doi: (<https://doi.org/10.351/7.0000180>).
- [142] G. Wang et al., "Process optimization and mechanical properties of oxide dispersion strengthened nickel-based superalloy by selective laser melting," *Materials & Design*, vol. 188, p. 108418, 2020, doi: (<https://doi.org/10.1016/j.matdes.2019.108418>).
- [143] Y. Bai, Y. Yang, Z. Xiao, M. Zhang, and D. Wang, Process optimization and mechanical property evolution of AlSiMgO. 75 by selective laser melting, *Materials & Design*, vol. 140, pp. 257–266, 2018, doi: <https://doi.org/10.1016/j.matdes.2017.11.045>.
- [144] Balbaa M, Mekhiali S, Elbestawi M, McIsaac J. On selective laser melting of Inconel 718: densification, surface roughness, and residual stresses. *Mater Des* 2020;vol. 193:108818. <https://doi.org/10.1016/j.matdes.2020.108818>.
- [145] H.S. Park, D.S. Nguyen, T. Le-Hong, and X. Van Tran, "Machine learning-based optimization of process parameters in selective laser melting for biomedical applications," *Journal of Intelligent Manufacturing*, pp. 1–16, 2021, doi: (<https://doi.org/10.1007/s10845-021-01773-4>).
- [146] E. Franczyk, M. Machno, and W. Zebala, Investigation and Optimization of the SLM and WEDM Processes' Parameters for the AlSi10Mg-Sintered Part, *Materials*, vol. 14, no. 2, p. 410, 2021, doi: (<https://doi.org/10.3390/ma14020410>).
- [147] Y. Wen et al., A novel experimental method for in situ strain measurement during selective laser melting. *Virtual and Physical Prototyping*, vol. 15, no. sup1, pp. 583–595, 2020, doi: (<https://doi.org/10.1080/17452759.2020.1842137>).
- [148] M. Narvan, A. Ghasemi, E. Fereiduni, S. Kendrishi, and M. Elbestawi, Part deflection and residual stresses in laser powder bed fusion of H13 tool steel, *Materials & Design*, vol. 204, p. 109659, 2021, doi: (<https://doi.org/10.1016/j.matdes.2021.109659>).
- [149] S. Waqar, K. Guo, and J. Sun, FEM analysis of thermal and residual stress profile in selective laser melting of 316L stainless steel, *Journal of Manufacturing Processes*, vol. 66, pp. 81–100, 2021, doi: (<https://doi.org/10.1016/j.jmapro.2021.03.040>).
- [150] Higashi M, Ozaki T. Selective laser melting of pure molybdenum: evolution of defect and crystallographic texture with process parameters. *Mater Des* 2020;191:108588. <https://doi.org/10.1016/j.matdes.2020.108588>.
- [151] D. Bayoumi, D. Schliephake, S. Dietrich, X. Wu, Y. Zhu, and A. Huang, Intensive processing optimization for achieving strong and ductile Al-Mn-Mg-Sc-Zr alloy produced by selective laser melting, *Materials & Design*, vol. 198, p. 109317, 2021, doi: (<https://doi.org/10.1016/j.matdes.2020.109317>).
- [152] H. Wan, Z. Zhou, C. Li, G. Chen, and G. Zhang, Effect of scanning strategy on grain structure and crystallographic texture of Inconel 718 processed by selective laser melting, *Journal of materials science & technology*, vol. 34, no. 10, pp. 1799–1804, 2018, doi: (<https://doi.org/10.1016/j.jmst.2018.02.002>).
- [153] L. Tonelli, A. Fortunato, and L. Ceschin, "CoCr alloy processed by Selective Laser Melting (SLM): effect of Laser Energy Density on microstructure, surface morphology, and hardness," *Journal of Manufacturing Processes*, vol. 52, pp. 106–119, 2020/04/01/ 2020, doi: (<https://doi.org/10.1016/j.jmapro.2020.01.052>).
- [154] X. Yin et al., "Effect of tungsten particles on microstructure and properties of 316 L stainless steel manufactured by selective laser melting," *Journal of Manufacturing Processes*, vol. 68, pp. 210–221, 2021/08/01/ 2021, doi: (<https://doi.org/10.1016/j.jmapro.2021.05.039>).
- [155] Q. Teng, S. Li, Q. Wei, and Y. Shi, "Investigation on the influence of heat treatment on Inconel 718 fabricated by selective laser melting: Microstructure and high temperature tensile property," *Journal of Manufacturing Processes*, vol. 61, pp. 35–45, 2021/01/01/ 2021, doi: (<https://doi.org/10.1016/j.jmapro.2020.11.002>).
- [156] K.C. Atli et al., "Laser-based additive manufacturing of a binary Ni-5 wt%Nb alloy," *Journal of Manufacturing Processes*, vol. 62, pp. 720–728, 2021/02/01/ 2021, doi: (<https://doi.org/10.1016/j.jmapro.2020.12.059>).
- [157] Z. Hu et al., "Top surface roughness evolution during selective laser melting of AlCu5MnCdVA aluminum alloy," *Journal of Manufacturing Processes*, vol. 64, pp. 1180–1195, 2021/04/01/ 2021, doi: (<https://doi.org/10.1016/j.jmapro.2021.01.051>).
- [158] M. Abdelhafiz, K.S. Al-Rubaie, A. Emadi, and M.A. Elbestawi, Process-Structure-Property Relationships of Copper Parts Manufactured by Laser Powder Bed Fusion, *Materials*, vol. 14, no. 11, p. 2945, 2021, doi: (<https://doi.org/10.3390/ma14112945>).
- [159] Weaver JS, et al. The effects of particle size distribution on the rheological properties of the powder and the mechanical properties of additively manufactured 17-4 PH stainless steel. 2021/03/01/ Addit Manuf 2021;39: 101851. <https://doi.org/10.1016/j.addma.2021.101851>.
- [160] Li J, Wei Z, Zhou B, Wu Y, Chen S-G, Sun Z. Densification, microstructure and properties of  $^{90}\text{W}-^7\text{Ni}-3\text{Fe}$  fabricated by selective laser melting. *Metals* 2019;9(8): 884. <https://doi.org/10.3390/met9080884>.
- [161] Cao Y, et al. Large tunable elastocaloric effect in additively manufactured Ni-Ti shape memory alloys. 2020/08/01/ *Acta Mater* 2020;194:178–89. <https://doi.org/10.1016/j.actamat.2020.04.007>.
- [162] Thapliyal S, et al. Design of heterogeneous structured Al alloys with wide processing window for laser-powder bed fusion additive manufacturing. 2021/06/01/ Addit Manuf 2021;42:102002. <https://doi.org/10.1016/j.addma.2021.102002>.
- [163] Z. Baicheng et al., "Study of selective laser melting (SLM) Inconel 718 part surface improvement by electrochemical polishing," *Materials & Design*, vol. 116, pp. 531–537, 2017/02/15/ 2017, doi: (<https://doi.org/10.1016/j.matdes.2016.11.103>).
- [164] M. Yakout, M.A. Elbestawi, and S.C. Veldhuis, "A study of thermal expansion coefficients and microstructure during selective laser melting of Invar 36 and stainless steel 316L," *Additive Manufacturing*, vol. 24, pp. 405–418, 2018/12/01/ 2018, doi: (<https://doi.org/10.1016/j.addma.2018.09.035>).
- [165] Liu J, et al. Achieving Ti6Al4V alloys with both high strength and ductility via selective laser melting. 2019/10/24/ *Mater Sci Eng: A* 2019;766:138319. <https://doi.org/10.1016/j.msea.2019.138319>.
- [166] X. Shi, C. Yan, W. Feng, Y. Zhang, and Z. Leng, "Effect of high layer thickness on surface quality and defect behavior of Ti-6Al-4V fabricated by selective laser melting," *Optics & Laser Technology*, vol. 132, p. 106471, 2020/12/01/ 2020, doi: (<https://doi.org/10.1016/j.optlastec.2020.106471>).
- [167] H.R. Javidrad, M. Ghanbari, and F. Javidrad, "Effect of scanning pattern and volumetric energy density on the properties of selective laser melting Ti-6Al-4V specimens," *Journal of Materials Research and Technology*, vol. 12, pp. 989–998, 2021/05/01/ 2021, doi: (<https://doi.org/10.1016/j.jmrt.2021.03.044>).
- [168] X.D. Nong and X.L. Zhou, "Effect of scanning strategy on the microstructure, texture, and mechanical properties of 15–5PH stainless steel processed by selective laser melting," *Materials Characterization*, vol. 174, p. 111012, 2021/04/01/ 2021, doi: (<https://doi.org/10.1016/j.matchar.2021.111012>).
- [169] J.W. Chen, C.H. Zhang, F.Q. Zhou, S. Zhang, H.T. Chen, and Q. Wang, "Microstructural, electrochemical and wear-corrosion characterization of TC4–5Cu alloy fabricated by selective laser melting," *Journal of Alloys and Compounds*, vol. 874, p. 159953, 2021/09/05/ 2021, doi: (<https://doi.org/10.1016/j.jallcom.2021.159953>).
- [170] Y. Zhang, A. Majeed, M. Muzamil, J. Lv, T. Peng, and V. Patel, "Investigation for macro mechanical behavior explicitly for thin-walled parts of AlSi10Mg alloy using selective laser melting technique," *Journal of Manufacturing Processes*, vol. 66, pp. 269–280, 2021/06/01/ 2021, doi: (<https://doi.org/10.1016/j.jmapro.2021.04.022>).
- [171] Zhou YH, et al. Selective laser melting of Ti–22Al–25Nb intermetallic: significant effects of hatch distance on microstructural features and mechanical properties. 2020/02/01/ *J Mater Process Technol* 2020;vol. 276:116398. <https://doi.org/10.1016/j.jmatprotec.2019.116398>.
- [172] Pal S, et al. Effect of the fabricating locations and orientations according to the powder coating direction in Selective Laser Melting on mechanical properties. 2021/07/01/ *Results Phys* 2021;vol. 26:104417. <https://doi.org/10.1016/j.rinp.2021.104417>.
- [173] Yang Q, et al. Compression and superelasticity behaviors of NiTi porous structures with tiny strut fabricated by selective laser melting. 2021/03/25/ *J Alloy Compd* 2021;vol. 858:157674. <https://doi.org/10.1016/j.jallcom.2020.157674>.
- [174] K.-S. Kim, S. Yang, M.-S. Kim, and K.-A. Lee, "Effect of post heat-treatment on the microstructure and high-temperature oxidation behavior of precipitation hardened IN738LC superalloy fabricated by selective laser melting," *Journal of Materials Science & Technology*, vol. 76, pp. 95–103, 2021/06/20/ 2021, doi: (<https://doi.org/10.1016/j.jmst.2020.11.013>).
- [175] S.-g. Chen, Y.-d. Zhang, Q. Wu, H.-j. Gao, Z.-h. Gao, and X. Li, "Effect of solid-state phase transformation on residual stress of selective laser melting Ti6Al4V," *Materials Science and Engineering: A*, vol. 819, p. 141299, 2021/07/05/ 2021, doi: <https://doi.org/10.1016/j.msea.2021.141299>.
- [176] Banhart J, Seeliger HW. Aluminium foam sandwich panels: manufacture, metallurgy and applications. *Adv Eng Mater* 2008;vol. 10(9):793–802. <https://doi.org/10.1002/adem.20080091>.
- [177] C. Chu, G. Graf, and D.W. Rosen, Design for additive manufacturing of cellular structures, *Computer-Aided Design and Applications*, vol. 5, no. 5, pp. 686–696, 2008, doi: (<https://doi.org/10.3722/cadaps.2008.686–696>).
- [178] Macaonchie T, et al. SLM lattice structures: properties, performance, applications and challenges. 2019/12/05/ *Mater Des* 2019;183:108137. <https://doi.org/10.1016/j.matdes.2019.108137>.
- [179] P. Wang, F. Yang, D. Ru, B. Zheng, and H. Fan, "Additive-manufactured hierarchical multi-circular lattice structures for energy absorption application," *Materials & Design*, vol. 210, p. 110116, 2021/11/15/ 2021, doi: (<https://doi.org/10.1016/j.matdes.2021.110116>).
- [180] W. Tao and M.C. Leu, "Design of lattice structure for additive manufacturing," in 2016 International Symposium on Flexible Automation (ISFA), 1–3 Aug. 2016 2016, pp. 325–332, doi: <https://doi.org/10.1109/ISFA.2016.7790182>.
- [181] C. Pan, Y. Han, and J. Lu, Design and Optimization of Lattice Structures: A Review, *Applied Sciences*, vol. 10, no. 18, p. 6374, 2020, doi: (<https://doi.org/10.3390/app10186374>).
- [182] C. Jing, Y. Zhu, J. Wang, F. Wang, J. Lu, and C. Liu, Investigation on Morphology and Mechanical Properties of Rod Units in Lattice Structures Fabricated by Selective Laser Melting, *Materials*, vol. 14, no. 14, p. 3994, 2021, doi: (<https://doi.org/10.3390/ma14143994>).
- [183] S. Liu and Y.C. Shin, "Additive manufacturing of Ti6Al4V alloy: A review," *Materials & Design*, vol. 164, p. 107552, 2019/02/15/ 2019, doi: (<https://doi.org/10.1016/j.matdes.2018.107552>).
- [184] P. Hanzl, M. Zetek, T. Bakša, and T. Kroupa, "The Influence of Processing Parameters on the Mechanical Properties of SLM Parts," *Procedia Engineering*, vol. 100, pp. 1405–1413, 2015/01/01/ 2015, doi: (<https://doi.org/10.1016/j.proeng.2015.01.510>).
- [185] T. Niendorf, F. Brenne, and M. Schaper, Lattice structures manufactured by SLM: on the effect of geometrical dimensions on microstructure evolution during processing, *Metallurgical and materials transactions B*, vol. 45, no. 4, pp. 1181–1185, 2014, doi: (<https://doi.org/10.1007/s11663-014-0086-z>).

- [186] M. Leary et al., "Selective laser melting (SLM) of AlSi12Mg lattice structures," *Materials & Design*, vol. 98, pp. 344–357, 2016/05/15/ 2016, doi: (<https://doi.org/10.1016/j.matdes.2016.02.127>).
- [187] B. Vandenbroucke and J.P. Kruth, Selective laser melting of biocompatible metals for rapid manufacturing of medical parts, *Rapid Prototyping Journal*, vol. 13, no. 4, pp. 196–203, 2007, doi: (<https://doi.org/10.1108/13552540710776142>).
- [188] A. Sarker et al., "Angle defines attachment: Switching the biological response to titanium interfaces by modifying the inclination angle during selective laser melting," *Materials & Design*, vol. 154, pp. 326–339, 2018/09/15/ 2018, doi: (<https://doi.org/10.1016/j.matdes.2018.05.043>).
- [189] L. Liu, P. Kamm, F. García-Moreno, J. Banhart, and D. Pasini, "Elastic and failure response of imperfect three-dimensional metallic lattices: the role of geometric defects induced by Selective Laser Melting," *Journal of the Mechanics and Physics of Solids*, vol. 107, pp. 160–184, 2017/10/01/ 2017, doi: (<https://doi.org/10.1016/j.jmps.2017.07.003>).
- [190] M.R. K Ravari et al., "On the effects of geometry, defects, and material asymmetry on the mechanical response of shape memory alloy cellular lattice structures," *Smart Materials and Structures*, vol. 25, no. 2, p. 025008, 2016/01/04 2016, doi: (<https://doi.org/10.1088/0964-1726/25/2/025008>).
- [191] H. Gong, K. Rafi, H. Gu, G.D. Janaki Ram, T. Starr, and B. Stucker, "Influence of defects on mechanical properties of Ti-6Al-4V components produced by selective laser melting and electron beam melting," *Materials & Design*, vol. 86, pp. 545–554, 2015/12/05/ 2015, doi: (<https://doi.org/10.1016/j.matdes.2015.07.147>).
- [192] C. Yan, L. Hao, A. Hussein, P. Young, and D. Raymont, "Advanced lightweight 316L stainless steel cellular lattice structures fabricated via selective laser melting," *Materials & Design*, vol. 55, pp. 533–541, 2014/03/01/ 2014, doi: (<https://doi.org/10.1016/j.matdes.2013.10.027>).
- [193] Y. Amani, S. Dancette, P. Delcroix, A. Simar, and E. Maire, "Compression behavior of lattice structures produced by selective laser melting: X-ray tomography based experimental and finite element approaches," *Acta Materialia*, vol. 159, pp. 395–407, 2018/10/15/ 2018, doi: (<https://doi.org/10.1016/j.actamat.2018.08.030>).
- [194] Campanelli SL, Contuzzi N, Ludovico AD, Caiazzo F, Cardaropoli F, Sergi V. Manufacturing and characterization of Ti6Al4V lattice components manufactured by selective laser melting. *Materials* 2014;7(6):4803–22. <https://doi.org/10.3390/ma7064803>.
- [195] T. Zhong, K. He, H. Li, and L. Yang, "Mechanical properties of lightweight 316L stainless steel lattice structures fabricated by selective laser melting," *Materials & Design*, vol. 181, p. 108076, 2019/11/05/ 2019, doi: (<https://doi.org/10.1016/j.matdes.2019.108076>).
- [196] S.L. Sing, F.E. Wirlia, and W.Y. Yeong, "Selective laser melting of lattice structures: A statistical approach to manufacturability and mechanical behavior," *Robotics and Computer-Integrated Manufacturing*, vol. 49, pp. 170–180, 2018/02/01/ 2018, doi: (<https://doi.org/10.1016/j.rcim.2017.06.006>).
- [197] A.A. Zadpoor, "Mechanical performance of additively manufactured meta-biomaterials," *Acta Biomaterialia*, vol. 85, pp. 41–59, 2019/02/01/ 2019, doi: (<https://doi.org/10.1016/j.actbio.2018.12.038>).
- [198] Bai L, Zhang J, Chen X, Yi C, Chen R, Zhang Z. Configuration optimization design of Ti6Al4V lattice structure formed by SLM. *Materials* 2018;11(10):1856. <https://doi.org/10.3390/ma11101856>.
- [199] Z.-h. Li, Y.-f. Nie, B. Liu, Z.-z. Kuai, M. Zhao, and F. Liu, "Mechanical properties of AlSi10Mg lattice structures fabricated by selective laser melting," *Materials & Design*, vol. 192, p. 108709, 2020/07/01/ 2020, doi: (<https://doi.org/10.1016/j.matdes.2020.108709>).
- [200] D. Kang, S. Park, Y. Son, S. Yeon, S.H. Kim, and I. Kim, "Multi-lattice inner structures for high-strength and light-weight in metal selective laser melting process," *Materials & Design*, vol. 175, p. 107786, 2019/08/05/ 2019, doi: (<https://doi.org/10.1016/j.matdes.2019.107786>).
- [201] Z. Ma, D.Z. Zhang, F. Liu, J. Jiang, M. Zhao, and T. Zhang, "Lattice structures of Cu-Cr-Zr copper alloy by selective laser melting: Microstructures, mechanical properties and energy absorption," *Materials & Design*, vol. 187, p. 108406, 2020/02/01/ 2020, doi: (<https://doi.org/10.1016/j.matdes.2019.108406>).
- [202] M. Leary et al., "Inconel 625 lattice structures manufactured by selective laser melting (SLM): Mechanical properties, deformation and failure modes," *Materials & Design*, vol. 157, pp. 179–199, 2018/11/05/ 2018, doi: (<https://doi.org/10.1016/j.matdes.2018.06.010>).
- [203] S.Y. Choy, C.-N. Sun, K.F. Leong, and J. Wei, "Compressive properties of Ti-6Al-4V lattice structures fabricated by selective laser melting: Design, orientation and density," *Additive Manufacturing*, vol. 16, pp. 213–224, 2017/08/01/ 2017, doi: (<https://doi.org/10.1016/j.addma.2017.06.012>).
- [204] Y. Xu et al., "Mechanical properties tailoring of topology optimized and selective laser melting fabricated Ti6Al4V lattice structure," *Journal of the Mechanical Behavior of Biomedical Materials*, vol. 99, pp. 225–239, 2019/11/01/ 2019, doi: (<https://doi.org/10.1016/j.jmbbm.2019.06.021>).
- [205] M. Mazur, M. Leary, S. Sun, M. Vcelka, D. Shidid, and M. Brandt, Deformation and failure behaviour of Ti-6Al-4V lattice structures manufactured by selective laser melting (SLM), *The International Journal of Advanced Manufacturing Technology*, vol. 84, no. 5, pp. 1391–1411, 2016, doi: (<https://doi.org/10.1007/s00170-015-7655-4>).
- [206] C. Yan, L. Hao, A. Hussein, and D. Raymont, "Evaluations of cellular lattice structures manufactured using selective laser melting," *International Journal of Machine Tools and Manufacture*, vol. 62, pp. 32–38, 2012/11/01/ 2012, doi: (<https://doi.org/10.1016/j.ijmachtools.2012.06.002>).
- [207] Bai L, et al. Quasi-Static compressive responses and fatigue behaviour of Ti-6Al-4 V graded lattice structures fabricated by laser powder bed fusion. 2021/11/15/ *Mater Des* 2021;210:11010. <https://doi.org/10.1016/j.matdes.2021.11010>.
- [208] D.S. J. Al-Saeed, S.H. Masood, M. Faizan-Ur-Rab, A. Alomarah, and P. Ponnusamy, "Mechanical properties and energy absorption capability of functionally graded F2BCC lattice fabricated by SLM," *Materials & Design*, vol. 144, pp. 32–44, 2018/04/15/ 2018, doi: (<https://doi.org/10.1016/j.matdes.2018.01.059>).
- [209] P. Piłatek, J. Sienkiewicz, J. Janiszewski, and F. Jiang, Investigations on Mechanical Properties of Lattice Structures with Different Values of Relative Density Made from 316L by Selective Laser Melting (SLM), *Materials*, vol. 13, no. 9, p. 2204, 2020, doi: (<https://doi.org/10.3390/ma13092204>).
- [210] B. Lozanovski et al., "Image-Based Geometrical Characterization of Nodes in Additively Manufactured Lattice Structures," *3D Printing and Additive Manufacturing*, vol. 8, no. 1, pp. 51–68, 2021, doi: (<https://doi.org/10.89/3dp.2020.0091>).
- [211] H. Lei et al., "Evaluation of compressive properties of SLM-fabricated multi-layer lattice structures by experimental test and  $\mu$ -CT-based finite element analysis," *Materials & Design*, vol. 169, p. 107685, 2019/05/05/ 2019, doi: (<https://doi.org/10.1016/j.matdes.2019.107685>).
- [212] M. Mazur, M. Leary, M. McMillan, S. Sun, D. Shidid, and M. Brandt, "5 - Mechanical properties of Ti6Al4V and AlSi12Mg lattice structures manufactured by Selective Laser Melting (SLM)," in *Laser Additive Manufacturing*, M. Brandt Ed.: Woodhead Publishing, 2017, pp. 119–161.
- [213] A. Ataei, Y. Li, M. Brandt, and C. Wen, "Ultrahigh-strength titanium gyroid scaffolds manufactured by selective laser melting (SLM) for bone implant applications," *Acta Materialia*, vol. 158, pp. 354–368, 2018/10/01/ 2018, doi: (<https://doi.org/10.1016/j.actamat.2018.08.005>).
- [214] H.E. Burton et al., "The design of additively manufactured lattices to increase the functionality of medical implants," *Materials Science and Engineering: C*, vol. 94, pp. 901–908, 2019/01/01/ 2019, doi: (<https://doi.org/10.1016/j.msec.2018.10.052>).
- [215] C. Yan, L. Hao, A. Hussein, and P. Young, "Ti-6Al-4V triply periodic minimal surface structures for bone implants fabricated via selective laser melting," *Journal of the Mechanical Behavior of Biomedical Materials*, vol. 51, pp. 61–73, 2015/11/01/ 2015, doi: (<https://doi.org/10.1016/j.jmbbm.2015.06.024>).
- [216] E. Saliccia-Leva, A.L. Jardini, and J.B. Fogagnolo, "Microstructure and mechanical behavior of porous Ti-6Al-4V parts obtained by selective laser melting," *Journal of the Mechanical Behavior of Biomedical Materials*, vol. 26, pp. 98–108, 2013/10/01/ 2013, doi: (<https://doi.org/10.1016/j.jmbbm.2013.05.011>).
- [217] M.X. Gan and C.H. Wong, "Practical support structures for selective laser melting," *Journal of Materials Processing Technology*, vol. 238, pp. 474–484, 2016/12/01/ 2016, doi: (<https://doi.org/10.1016/j.jmatprotec.2016.08.006>).
- [218] J.-P. Järvinen et al., "Characterization of Effect of Support Structures in Laser Additive Manufacturing of Stainless Steel," *Physics Procedia*, vol. 56, pp. 72–81, 2014/01/01/ 2014, doi: (<https://doi.org/10.1016/j.phpro.2014.08.099>).
- [219] J. Jiang, X. Xu, and J. Stringer, Support structures for additive manufacturing: a review, *Journal of Manufacturing and Materials Processing*, vol. 2, no. 4, p. 64, 2018, doi: (<https://doi.org/10.3390/jmmp2040064>).
- [220] F. Calignano, "Design optimization of supports for overhanging structures in aluminum and titanium alloys by selective laser melting," *Materials & Design*, vol. 64, pp. 203–213, 2014/12/01/ 2014, doi: (<https://doi.org/10.1016/j.matdes.2014.07.043>).
- [221] Li Z, Zhang DZ, Dong P, Kucukkoc I. A lightweight and support-free design method for selective laser melting. *Int J Adv Manuf Technol* 2017;90(9–12): 2943–53. <https://doi.org/10.1007/s00170-016-9509-0>.
- [222] K. Cooper, P. Steele, B. Cheng, and K. Chou, Contact-free support structures for part overhangs in powder-bed metal additive manufacturing, *Inventions*, vol. 3, no. 1, p. 2, 2018, doi: (<https://doi.org/10.3390/inventions3010002>).
- [223] Q. Cao et al., "A novel method to improve the removability of cone support structures in selective laser melting of 316L stainless steel," *Journal of Alloys and Compounds*, vol. 854, p. 157133, 2021/02/15/ 2021, doi: (<https://doi.org/10.1016/j.jallcom.2020.157133>).
- [224] Y. Kaynak and O. Kitay, "The effect of post-processing operations on surface characteristics of 316L stainless steel produced by selective laser melting," *Additive Manufacturing*, vol. 26, pp. 84–93, 2019/03/01/ 2019, doi: (<https://doi.org/10.1016/j.addma.2018.12.021>).
- [225] Boschetto A, Bottini L, Macera L, Veniali F. Post-processing of complex SLM parts by barrel finishing. *Appl Sci* 2020;10(4):1382. (<https://doi.org/10.3390/app10041382>).
- [226] Karami K, et al. Continuous and pulsed selective laser melting of Ti6Al4V lattice structures: effect of post-processing on microstructural anisotropy and fatigue behaviour. 2020/12/01/ *Addit Manuf* 2020;vol. 36:101433. <https://doi.org/10.1016/j.addma.2020.101433>.
- [227] A.H. Maamoun, M. Elbestawi, G.K. Dosbaeva, and S.C. Veldhuis, "Thermal post-processing of AlSi10Mg parts produced by Selective Laser Melting using recycled powder," *Additive Manufacturing*, vol. 21, pp. 234–247, 2018/05/01/ 2018, doi: (<https://doi.org/10.1016/j.addma.2018.03.014>).
- [228] H. Zhang, D. Dong, S. Su, and A. Chen, "Experimental study of effect of post processing on fracture toughness and fatigue crack growth performance of selective laser melting Ti-6Al-4V," *Chinese Journal of Aeronautics*, vol. 32, no. 10, pp. 2383–2393, 2019/10/01/ 2019, doi: (<https://doi.org/10.1016/j.cja.2018.12.007>).
- [229] X. Peng, L. Kong, J.Y. H. Fuh, and H. Wang, A Review of Post-Processing Technologies in Additive Manufacturing, *Journal of Manufacturing and Materials Processing*, vol. 5, no. 2, p. 38, 2021, doi: (<https://doi.org/10.3390/jmmp5020038>).

- [230] Markopoulos AP. "Finite Elem Method Mach Process," 2012.
- [231] T. Mayer, G. Brändle, A. Schönenberger, and R. Eberlein, Simulation and validation of residual deformations in additive manufacturing of metal parts, *Heliyon*, vol. 6, no. 5, p. e03987, 2020, doi: <https://doi.org/10.1016/j.heliyon.2020.e03987>.
- [232] Pagac M, et al. Prediction of model distortion by FEM in 3D printing via the selective laser melting of stainless steel AISI 316L. *Appl Sci* 2021;11(4):1656. <https://doi.org/10.3390/app11041656>.
- [233] Xing W, Ouyang D, Li N, Liu L. Estimation of residual stress in selective laser melting of a zr-based amorphous alloy. *Materials* 2018;11(8):1480. <https://doi.org/10.3390/ma11081480>.
- [234] Yilmaz N, Kayacan MY. Effect of single and multiple parts manufacturing on temperature-induced residual stress problems in SLM. *Int J Mater Form* 2020; 1–13. <https://doi.org/10.1007/s12289-020-01560-1>.
- [235] Peter N, Pitts Z, Thompson S, Saharan A. Benchmarking build simulation software for laser powder bed fusion of metals. *Addit Manuf* 2020;36:101531. <https://doi.org/10.1016/j.addma.2020.101531>.
- [236] M. Yakout and M. Elbestawi, "Residual Stress Formation in Laser-Based Powder Bed Fusion (PBF-LB) of Invar 36," *Structural Integrity of Additive Manufactured Materials and Parts*, pp. 34–44, 2020, doi: <https://doi.org/10.1520/STP163120190149>.
- [237] P. Ninpitch, P. Kowitwarangkul, S. Mahathanabodee, P. Chalermkarnnon, and P. Ratanadecho, "A review of computer simulations of metal 3D printing," in *AIP Conference Proceedings*, (2020), vol. 2279, no. 1: AIP Publishing LLC, p. 050002, doi: <https://doi.org/10.1063/5.0022974>.
- [238] Zongo F, Simoneau C, Timercan A, Tahhan A, Brailovski V. Geometric deviations of laser powder bed-fused AlSi10Mg components: numerical predictions versus experimental measurements. *Int J Adv Manuf Technol* 2020;107(3):1411–36. <https://doi.org/10.1007/s00170-020-04987-7>.
- [239] Khaimovich A, Stepanenko I, Smelov V. Optimization of selective laser melting by evaluation method of multiple quality characteristics (in). *IOP Conference Series: Materials Science and Engineering*, 302. IOP Publishing, 2018. <https://doi.org/10.1088/1757-899X/302/1/012067>.
- [240] S. Jonsson and S. Krappadal, "Evaluation of residual stresses and distortions in additively manufactured components," ed, 2018.
- [241] Huo Y-s, Hong C, Li H-x, Liu P. Influence of different processing parameter on distortion and residual stress of inconel 718 alloys fabricated by selective laser melting (SLM). *Mater Res* 2020;23(6). <https://doi.org/10.1590/1980-5373-MR-2020-0176>.
- [242] Singh SN, et al. A comparative analysis of laser additive manufacturing of high layer thickness pure Ti and Inconel 718 alloy materials using finite element method. *Materials* 2021;14(4):876. <https://doi.org/10.3390/ma14040876>.
- [243] Li C, Liu J, Fang X, Guo Y. Efficient predictive model of part distortion and residual stress in selective laser melting. *Addit Manuf* 2017;17:157–68. <https://doi.org/10.1016/j.addma.2017.08.014>.
- [244] Y. Woo, T. Hwang, I. Oh, D. Seo, and Y. Moon, "Analysis on selective laser melting of WC-reinforced H13 steel composite powder by finite element method," *Advances in Mechanical Engineering*, vol. 11, no. 1, p. 1687814018822200, 2019, doi: <https://doi.org/10.1177/1687814018822200>.
- [245] A. Cardon, C. Mareau, Y. Ayed, S. Van Der Veen, E. Giraud, and P. Dal Santo, "Heat treatment simulation of Ti-6Al-4V parts produced by selective laser melting," *Additive Manufacturing*, vol. 39, p. 101766, 2021/03/01/ 2021, doi: <https://doi.org/10.1016/j.addma.2020.101766>.
- [246] J. Wu, L. Wang, and X. An, "Numerical analysis of residual stress evolution of AlSi10Mg manufactured by selective laser melting," *Optik*, vol. 137, pp. 65–78, 2017/05/01/ 2017, doi: <https://doi.org/10.1016/j.ijleo.2017.02.060>.
- [247] Minetola P, Stiuso V, Calignano F, Galati M, Khandpur M, Fontana L. "Experimental validation of laser powder bed fusion simulation," in: *IOP Conference Series: Materials Science and Engineering*, 1091. IOP Publishing, 2021.
- [248] K.H. Leitz, P. Singer, A. Plankenstein, B. Tabernig, H. Kestler, and L.S. Sigl, "Multi-physical simulation of selective laser melting," *Metal Powder Report*, vol. 72, no. 5, pp. 331–338, 2017/09/01/ 2017, doi: <https://doi.org/10.1016/j.mprp.2016.04.004>.
- [249] S. Afazov, W.A. D. Denmark, B. Lazaro Toralles, A. Holloway, and A. Yaghie, "Distortion prediction and compensation in selective laser melting," *Additive Manufacturing*, vol. 17, pp. 15–22, 2017/10/01/ 2017, doi: <https://doi.org/10.1016/j.addma.2017.07.005>.
- [250] X. Li, H.J. Willy, S. Chang, W. Lu, T.S. Herring, and J. Ding, "Selective laser melting of stainless steel and alumina composite: Experimental and simulation studies on processing parameters, microstructure and mechanical properties," *Materials & Design*, vol. 145, pp. 1–10, 2018/05/05/ 2018, doi: <https://doi.org/10.1016/j.matdes.2018.02.050>.
- [251] R. Sharma and A. Kumar, Track-Scale Simulations of Selective Laser Melting to Investigate Development and Mitigation of Thermal Stresses, *Lasers in Manufacturing and Materials Processing*, vol. 6, no. 4, pp. 464–492, 2019, doi: <https://doi.org/10.1007/s40516-019-00103-0>.
- [252] W. Ye et al., "Numerical simulation of the melting and alloying processes of elemental titanium and boron powders using selective laser alloying," *Journal of Manufacturing Processes*, vol. 64, pp. 1235–1247, 2021/04/01/ 2021, doi: <https://doi.org/10.1016/j.jmapro.2021.02.044>.